Turbine Tip Clearance Loss Mechanisms

by

Steven Mazur

Submitted to the Department of Aeronautics and Astronautics
in partial fulfillment of the requirements for the degree of

Master of Science in Aeronautics and Astronautics

at the

MASSACHUSETTS INSTITUTE OF TECHNOLOGY

June 2013

Author .....
Department of Aeronautics and Astronautics
May 28, 2013

Certified by .....
Edward M. Greitzer
H.N. Slater Professor of Aeronautics and Astronautics
Thesis Supervisor

Certified by .....
Choon S. Tan
Senior Research Engineer
Thesis Supervisor

Certified by .....
Steven Gegg
Manager, Turbine Aerodynamics, Rolls-Royce Corporation
Thesis Supervisor

Accepted by .....
Etyan H. Modiano
Professor of Aeronautics and Astronautics
Chair, Graduate Program Committee

Turbine Tip Clearance Loss Mechanisms

by

Steven Mazur

Submitted to the Department of Aeronautics and Astronautics
on May 28, 2013, in partial fulfillment of the
requirements for the degree of
Master of Science in Aeronautics and Astronautics

Abstract

Three-dimensional numerical simulations (RANS and URANS) were used to assess the impact of two specific design features, and of aspects of the actual turbine environment, on turbine blade tip loss. The calculations were carried out for a subsonic high pressure turbine stage. The loss mechanism examined is that due to tip clearance vortex mixing. The effects examined were three-dimensional blade stacking, downstream transition duct geometry, and unsteadiness due to an upstream nozzle guide vane. Tip leakage loss changes due to three-dimensional blade stacking (bowing or reverse bowing) are verified to be associated with changes in the magnitude of blade tip loading, which create differences in the leakage flow exit velocities. The effect of a downstream diffusing transition duct on tip leakage losses is small; there was a 3.6% increase in tip leakage loss for a 65% increase in duct exit-to-inlet area ratio compared to a constant area duct. For unsteadiness arising from an upstream nozzle guide vane, it is shown that substantial temporal fluctuations in vortex core velocity and loss generation exist. However, the time average tip leakage loss differed less than 5% from the tip leakage loss calculated on a steady flow basis. Based on the computations, the mechanism for tip leakage vortex loss in the three different situations examined appears to be similar to that which is seen for an isolated turbine blade.

Thesis Supervisor: Edward M. Greitzer
Title: H.N. Slater Professor of Aeronautics and Astronautics

Thesis Supervisor: Choon S. Tan
Title: Senior Research Engineer

Thesis Supervisor: Steven Gegg
Title: Manager, Turbine Aerodynamics, Rolls-Royce Corporation

Acknowledgments

This research is done with the support of the Rolls-Royce Whittle Fellowship and the work herein represents a close collaboration between the MIT Gas Turbine Lab and the Turbine Aerodynamics group at Rolls-Royce.

This work would not have been possible without the help of my advisors, Professor Greitzer and Dr. Choon Tan. Their guidance and insight helped me press on when the path forward was far from obvious. I would like to thank Arthur Huang as well, the previous Rolls-Royce Whittle Fellow. The entire process from start to finish would have been much more difficult without his help in setting up and analyzing the CFD results.

I would also like to thank the engineers of the Rolls-Royce Turbine Aerodynamics group. In particular, Steve Gegg, Ed Turner, and Eugene Clemens offered their help without hesitation through the course of this thesis and it was invaluable to its completion. In addition, members of the Rolls-Royce Methods group, Todd Simons, Kurt Weber, and Moujin Zhang, provided many hours of help in implementing HYDRA for my research.

I would like to express my gratitude to my fellow labmates, their support was helpful to the completion of this thesis. The GTL is an environment which encourages sharing of ideas to further research and understanding, and it proved valuable over the last two years.

My family has helped me become who I am today, and I am very thankful for their support. Lastly I would like to thank Megan. You always believed in me even when I didn't, and have been the rock that I needed during this process. I could not have done it without you.

Contents

List of Figures

List of Tables

Nomenclature

$\bar{L}$	Average Transition Duct Wall Length
β	Reduced Frequency
ΔR_d	Transition Duct Inlet Span
Δu	Difference Between Vortex Core and Freestream Velocities
$\dot{m}_{main}$	Mainstream Flow
$\dot{m}_{tip}$	Tip Leakage Flow
ϵ	Leakage Angle
Γ	Circulation $= \int \omega dA$
μ_{eff}	Effective Viscosity
Ω	Blade Rotational Speed
ω	Vorticity
Ω_{ij}	Mean Rate-of-Rotation Tensor
ϕ	Flow Coefficient $= \frac{v_x}{\Omega r}$
ψ	Work Coefficient $= \frac{\Delta h_t}{(\Omega r)^2}$
ρ	Density
σ	Solidity

ξ	Loss Coefficient
AR	Exit-to-Inlet Area Ratio
c	Blade Chord
C_d	Gap Coefficient of Discharge
C_p	Non-dimensional Pressure Rise
c_p	Constant Pressure Specific Heat
c_p^*	Ducts that give maximum pressure recovery for a given non-dimensional length
c_p^{**}	Ducts that give maximum pressure recovery for a given area ratio
D_h	Hydraulic Diameter
g	Tip Clearance Height
M	Mach Number
p	Pressure
p_t	Stagnation Pressure
q	Dynamic Pressure: $1/2\rho U^2$
Re	Reynolds Number
S	Spalart Allmaras Turbulence Production Term
S	Swirl Number $= v_\theta/u$
s	Specific Entropy
S_{ij}	Mean Strain Rate Tensor
T	Temperature
t	Time

T_t Stagnation Temperature

t_{vane} Vane Passing Period

u, U Wake or Average Core Velocity, Freestream Velocity

u, v, w velocity components in the x,y,z directions respectively

v_θ Swirl Velocity

VR Velocity Ratio = $\frac{u}{U}$

x, r, θ Cylindrical Coordinates

x, y, z Cartesian Coordinates

x/c Axial Distance Normalized by Blade Chord

y^+ Non-dimensional Wall Cell Distance

FL Forward Blade Loading Style

ML Middle Blade Loading Style

Chapter 1

Introduction

Turbomachines have clearance gaps between the rotating blade tips and the stationary casing. The losses generated due to leakage flow through this gap are approximately linearly proportional to the gap height. The magnitude of this proportionality, referred to as the leakage loss slope, depends on the blade design.

Rotating blades can either be of the shrouded or unshrouded type. Shrouded blades carry a portion of the endwall at the blade tips that forms a seal with the outer casing. Unshrouded blades have a gap between the tip and the casing, with flow forced from pressure side to suction side through the gap by the pressure difference across the tip. The leakage flow generates losses both inside the gap and in mixing with the mainstream flow. Unshrouded turbine blades are the subject of this thesis.

1.1 Background

Turbine tip leakage flows account for about one third of the total turbine stage loss [7]. For a given blade design, this loss grows roughly linearly with tip gap height and has a penalty of one to three percent or more of stage efficiency for a gap height equal to 1% blade span [1]. The overtip flow can also enhance heat transfer in the tip region.

The flow through the gap can be modeled as a vena contracta with a coefficient of discharge. There is a separation bubble present if the pressure side gap corner is

sharp. The flow reattaches before exiting the gap if the blade tip thickness is greater than roughly four times the gap height [3]. Two-dimensional sketches of the leakage flow are shown in Figure 1-1 for cases in which the flow does and does not reattach before exiting the gap. In the thick blade case, the flow mixes and reattaches such that the separation bubble does not extend the entire blade thickness as in the thin blade case. In both sketches, the vortex and its sense of rotation is shown on the suction side of the blade passage.

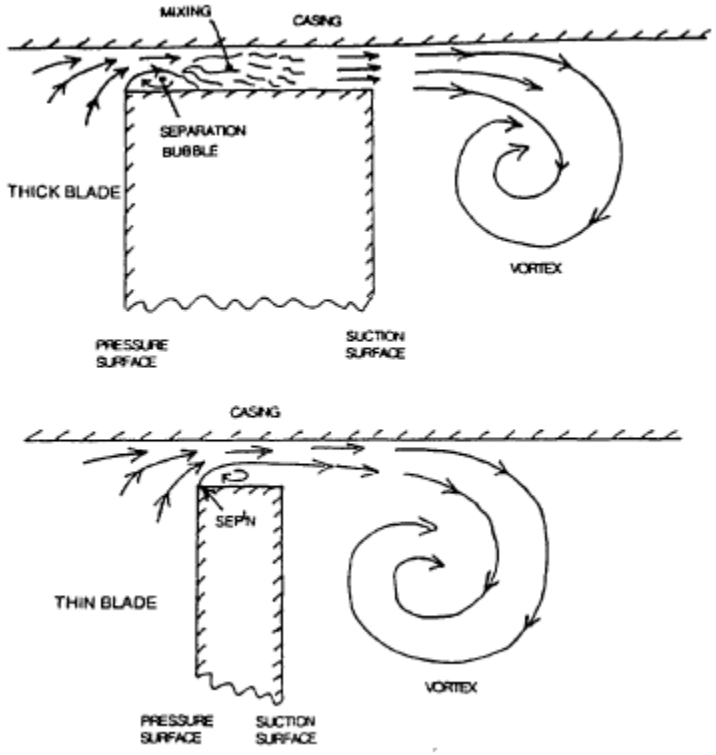

Figure 1-1: Flow over tip gap for unshrouded blade, $r - \theta$ plane looking aft a)Thick Blade, b)Thin Blade [3]

Most of the loss generation associated with the tip leakage flow is due to mixing with the freestream flow; for turbines only 15% of the tip leakage loss is generated within the gap itself [10]. On the suction side of the passage, the flow forms a shear layer due to the difference in velocity with the main passage flow. This layer rolls up, forming a tip leakage vortex. The details of how the vortex changes as it develops and moves downstream are influenced by blade tip design, blade design, and design

of the downstream diffusing ducts.

Several models have been developed to predict the gap exit massflow, velocity profiles, and loss generated due to mixing with the freestream. Heyes and Hodson estimate the leakage angle of the gap exit flow using a control volume approach that models the behavior of the flow as a vena contracta followed by mixing before the flow exits the gap. Their results showed good agreement with turbine cascade data [8]. Sjolander viewed loss generation during mixing with the mainstream flow as due to dissipation of the kinetic energy associated with the normal gap exit velocity [10], and matched experimental cascade tip loss data for gap thickness to blade chord ratios of 0.015 and 0.02 closely with their loss model. Denton developed estimates for the total mixing loss generated which account for the difference in axial velocity of the gap exit flow, in addition to the normal gap exit velocity. Denton assumed the flow mixes immediately with the freestream flow at constant pressure [3]. Huang evaluated the Denton model for a simple channel with mass injection through a slot and found it to be accurate within $\pm$ 40%, with the deviation being the largest when vortex contraction or stretching were present [9].

Huang showed that the behavior of the tip leakage flow in turbines is different from compressors because of stronger swirl. As a result of high swirl the turbine tip leakage loss can decrease with mainstream pressure rise increase, until vortex breakdown, at which further pressure rise increases the mixing loss. In the high pressure unshrouded turbine blades of interest in this thesis, the tip leakage vortex undergoes breakdown, and the severity of the breakdown is an important mechanism for the tip leakage loss generation [9]. Applying these ideas to turbine airfoil design, Huang was able to reduce tip leakage loss by 16% through reducing the trailing edge diffusion [9].

The work of Huang and others focused on a blade row in isolation, but this is not the real environment in which a turbine blade operates. Turbine blades are typically embedded within upstream and/or downstream transition ducts and vanes which can affect the blade aerodynamics. In addition, the turbine operates in an unsteady environment, while much of the work referred to above assumes steady flow. In order to use the prior work to effectively design turbine blade rows, the real turbine

environment impacts must be assessed, and that goal is the focus of this work.

1.2 Research Questions

The aim of this work is to quantify the impact of turbine design factors such as three-dimensional blade design, the design of the downstream transition duct, and the presence of unsteadiness from an upstream vane on tip leakage loss generation mechanisms. Specific research questions are:

- What is the impact of turbine blade bow on the tip clearance loss?
- How does the downstream transition duct affect tip loss mechanisms?
- Does the vortex mixing loss mechanism described by Huang hold in unsteady flow due to the presence of an upstream vane?

1.3 Methodology

Three-dimensional computations have been used to address the above questions. The work focuses on the mixing out of the leakage flow because this is the major cause of leakage loss. The impact of changing blade tip geometry, and of adjacent flow path geometry parameters, on tip leakage loss was determined. The important flow features were identified through these numerical analyses.

1.4 Contributions

- The effect of blade bowing on tip loss mechanisms has been described. Bowing is shown to change the magnitude of blade tip loading and thus the difference between tip leakage gap exit velocity and blade suction side freestream velocity. For positive bowing there is a reduction in this difference and hence in the leakage flow mixing losses.

- Over the range examined, the effect of the downstream diffusing transition duct design on tip leakage losses is small. A 65% increase in duct area ratio caused a 3.6% increase in tip loss coefficient. The implication is that the downstream diffusing transition duct can be designed to meet other constraints without creating large increases in tip loss.

- The time average tip leakage loss, calculated using URANS, with unsteadiness arising from the upstream nozzle guide vane, differed less than 5% from tip leakage loss calculated on a steady state basis. The time average blade loading, leakage flow, and vortex core velocity also show little change from those as given by steady state calculations. Further, model calculations with an axisymmetric vortex in a pressure rise show the tip leakage loss vortex breakdown mechanism is insensitive to unsteady pressure fluctuations. This implies that steady calculations predict the tip loss coefficient trends adequately.

- The reduced frequency in the vortex core was 0.8. The flow through the tip gap, however, is characterized by a reduced frequency less than 0.1, and can be treated as quasi-steady, as verified by comparison of quasi-steady gap flow analyses.

- Although the time average quantities match the steady values, there are substantial instantaneous fluctuations in the vortex flow field. The vortex core velocity at the blade trailing edge changes by $\pm 15\%$ over the period, which causes variation in the dissipation associated with vortex breakdown of $\pm 20\%$ over the period.

1.5 Organization of Thesis

Chapter 2 describes the approach and the design of computations to address the three research questions posed. Chapter 3 describes the behavior of bowed blades and the physical connection between bowing and tip loss. In Chapter 4 the effect of downstream transition duct design on the tip leakage loss is assessed. In Chapter

5 the time average effect of unsteadiness due to an upstream nozzle guide vane on the tip loss is determined along with a description of the time average flow behavior. Chapter 6 presents the temporal effects of unsteadiness for the nozzle guide vane-blade interaction. An unsteady axisymmetric vortex model problem is also examined to provide insight into the time average results of Chapter 5. Finally, Chapter 7 gives conclusions and recommendations for future work.

Chapter 2

Assessing Tip Flow Effects in the Turbine Environment

2.1 Introduction

This chapter describes flow features that result from the presence of a tip clearance gap and the approach for assessing their impact on loss. Based on prior work, several effects were hypothesized to be important in the context of the research questions posed in Chapter 1. In addressing the questions, it is useful to consider the flow in two conceptual "pieces": the flow that exits the gap, and the flow subsequent to this exit, in particular the vortex that develops and then mixes with the freestream. The effects are illustrated using three-dimensional turbine airfoil calculations.

The analysis metrics introduced in this chapter are applied in subsequent chapters to assess impacts on the tip leakage loss. Specifically, the leakage flow is characterized by the axial distribution of the mass flow exiting the gap, and the angle between the leakage flow and the freestream flow. The vortex is characterized by the ratio of streamwise velocity in the core to freestream velocity (in the core axis direction) and the swirl number, the ratio of the swirl velocity to average streamwise velocity in the core. The axial distribution of loss generation due to vortex mixing is also found to be important in determining the locations in the flow field that are critical to overall loss generation.

2.2 Computational Methodology

To examine the loss due to tip clearance flow, two separate calculations were run for each effect to be studied. One has no tip gap clearance, referred to as the 0% clearance case. The other has a (radial) tip gap of 2% of the blade height, referred to as the 2% case. The calculations were done for isolated blades, blades with downstream turbine transition ducts, and a vane-blade (stage) configuration. In this last situation the flow was unsteady.

FINE^{TM}/Turbo was initially selected for its structured tip gap mesh capability, but the decision was made to move to the Rolls-Royce proprietary CFD code HYDRA in order to work more effectively with Rolls-Royce. Investigations of the bowed blade and transition duct effects were done using NUMECA FINE^{TM}/Turbo, while the subsequent studies were done using HYDRA. Structured meshes were used in both cases, an example of which is shown in Figure 2-1. The HYDRA solver is unstructured while the FINE^{TM}/Turbo solver is structured. The HYDRA Spallart-Allmaras (SA) turbulence model uses a rotational correction so it diffuses the vortex core to a lesser extent than the FINE^{TM}/Turbo SA turbulence model. The effects of turbulence model on the computed details of the leakage loss mechanisms are described at the end of this chapter.

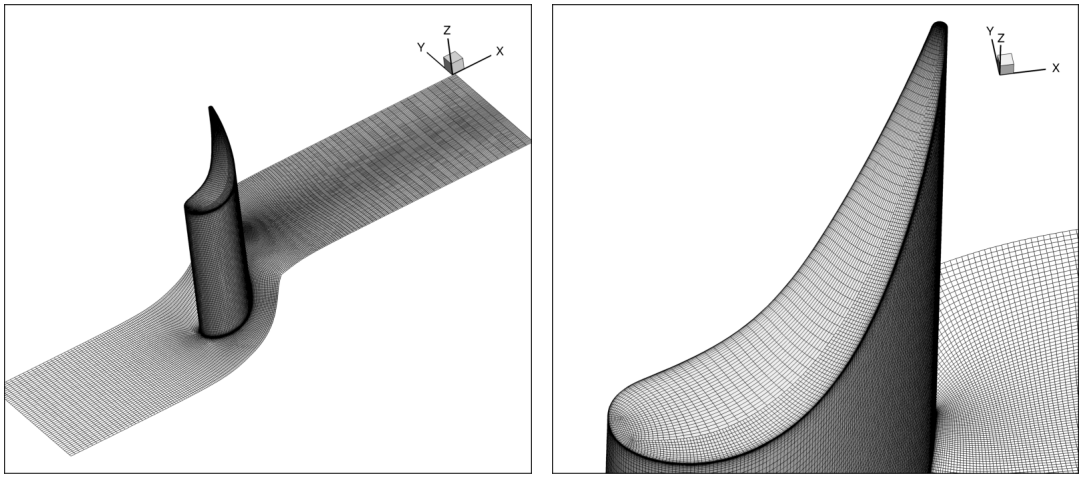

(a) (b)

Figure 2-1: Typical Grid Geometry: a)Mesh of hub and blade, b)Tip mesh

The inlet boundary conditions enforced are radial distributions of stagnation pressure, stagnation temperature, turbulent viscosity, and inlet flow angle. The outlet boundary condition is the radial distribution of static pressure that satisfies radial equilibrium with the pressure specified at the hub radius. All walls were enforced to be no-slip and adiabatic. The casing was stationary. Both solvers used the Reynolds-Averaged Navier Stokes (RANS) equations, and the unsteady calculations were done in HYDRA with the unsteady RANS (URANS) equations. All meshes had an average y^+ of 1 to resolve the boundary layers. The SA turbulence model was used with an initial turbulent to laminar viscosity ratio of 100 to represent the high turbulence level of the flow exiting the combustor, although it was shown by Huang that the results concerning tip loss are insensitive to the inlet turbulent viscosity ratio [9]. The parameters describing the turbine used in this study are shown in Table 2.1

Work Coefficient	2.13
Flow Coefficient	0.584
Midspan Relative Inlet Angle	54.3°
Midspan Relative Exit Angle	64.6°
Exit Mach Number	0.755
Stagnation-to-Static Pressure Ratio	2.22
Solidity	0.966
Aspect Ratio	1.25
Exit Relative Re_c	3.8 x 10^6

Table 2.1: Turbine Parameters

2.2.1 Blade Design Specification

Two main blade designs are examined in this work. The difference between the two blades is the tip airfoil shape, which is blended into a geometry that is identical for both blades from 0% to 50% span. The shape differences result in pressure loading differences between the two blades in the near tip region. The designs were created to highlight the loss mechanism shown by Huang, in which loss generation due to leakage flow was found to be sensitive to the pressure rise encountered by the tip leakage vortex [9].

The baseline blade has a mid loading (ML Blade), and the blade that reduces the pressure rise encountered by the leakage flow is the forward loaded blade (FL Blade). The two tip airfoil designs and resulting near tip blade loadings are shown in Figure 2-2. The axial location in this thesis is normalized by blade chord, with x/c = 0 corresponding to the blade leading edge, and x/c = 1 corresponding to the blade trailing edge.

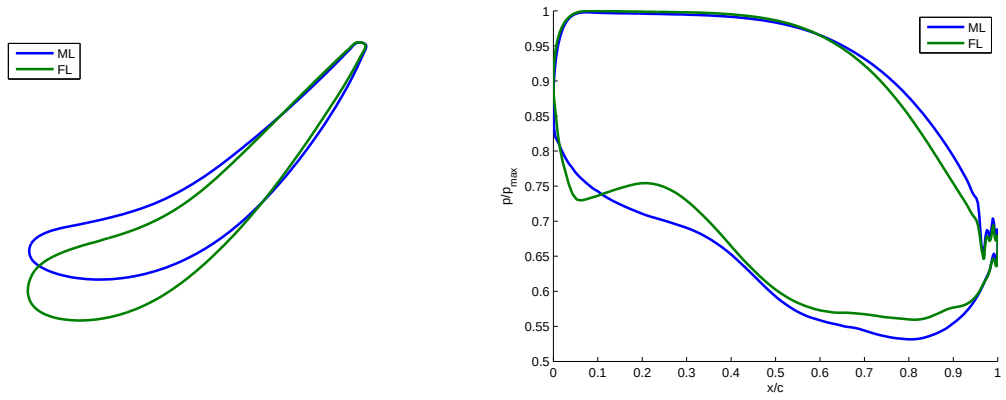

(a) (b)

Figure 2-2: ML and FL Blade Definitions: a)Tip Airfoil Geometry [9], b)Pressure Distribution at 85% span

2.3 Tip Leakage Vortex Characteristics and Description

The focus of this work is the tip leakage vortex that forms near the suction side of the blade passage. We define the vortex core as the flow field region with positive relative streamwise vorticity.

The vortex is characterized by a shear layer that exits the tip gap and rolls up into a vortex. Flow field quantities illustrating the roll up are shown on several slices, at different streamwise positions, in Figure 2-3. Figure 2-3(a) shows the development of the streamwise vorticity, vorticity aligned with the mean freestream velocity vector, in the vortex core. As the vortex is convected downstream, the shear layer adds

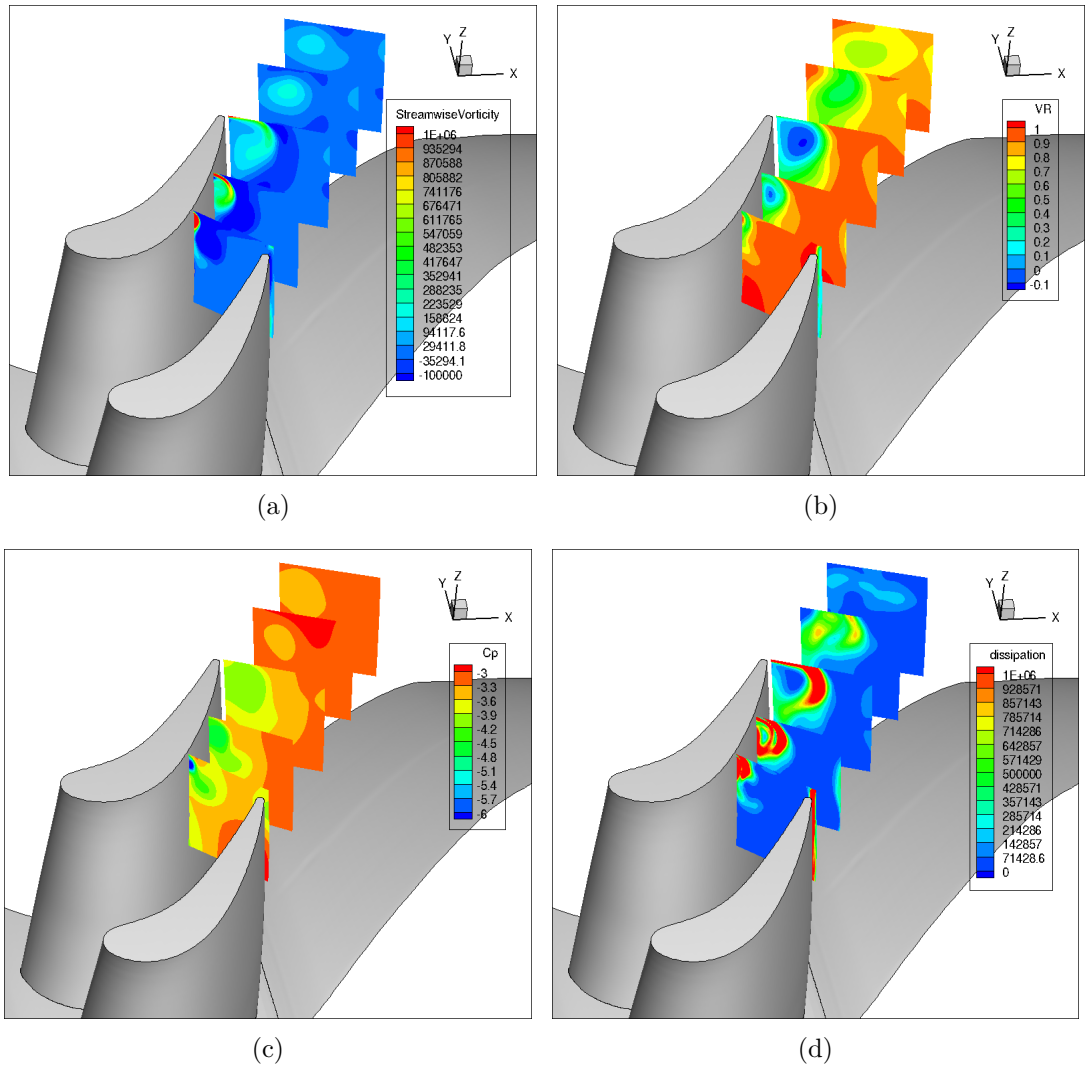

(a) (b)

(c) (d)

Figure 2-3: Tip Leakage Vortex Slices at x/c = 0.66, 0.81, 0.97, 1.20, 1.41 : a)Streamwise Vorticity, b)Streamwise Velocity, c)Pressure Field, d)Dissipation

circulation to the vortex, which grows in size. The result is a strongly swirling motion with a low pressure region in the center of the vortex as seen in the slice at x/c = 0.66 in Figure 2-3(c). As a result of the swirl and the low core velocity (compared to freestream), the response of the vortex core velocity to the external pressure rise is larger than that of the external flow as shown in Figure 2-3(b). The entropy generation, or dissipation, shown in Figure 2-3(d), is greatest near the axial location where the core velocity is lowest, at x/c = 1.1.

The external pressure gradients to which the vortex core is subjected depend on the blade tip geometry. Trailing edge diffusion decelerates the core, from x/c = 0.7 to x/c = 1 in the particular turbine studied. The flow on the centerline reacts more strongly to the pressure rise than the freestream and, if the deceleration is strong enough, vortex breakdown occurs [9].

2.4 Vortex Breakdown

Vortex breakdown, characterized by the stagnation and reversal of flow in the center of the vortex core, is due to the core being subjected to a pressure rise. The magnitude of the external pressure rise that causes the onset of flow reversal is lower for swirling flow than it is for non-swirling flow. The vortex core has increased sensitivity to external streamwise pressure gradients due to radial pressure gradients in the core. This is illustrated by Equation 2.1, which gives an estimate of the difference in axial pressure gradient between core edge and core centerline due to vortex core radius increase [6]. The core axis pressure gradient is larger than the edge external pressure gradient by a factor proportional to Γ^2, and the core axis velocity response is amplified as a result.

$$\left.\frac{\partial p}{\partial x}\right|_{r=0} - \frac{dp_{r_e}}{dx} = \rho \frac{\Gamma^2}{4\pi^2 r_e^3} \frac{dr_e}{dx} \tag{2.1}$$

In reference [9], a 7% reduction in leakage loss was obtained by redesigning the tip to reduce the pressure rise near the trailing edge and thus reduce the severity of the vortex breakdown. The ML blade was the baseline blade geometry in that work,

while the FL blade reduced the trailing edge pressure rise to achieve the leakage loss reduction.

An indication of the vortex breakdown severity, and the loss generated due to the breakdown, is the size of the flow reversal region which is shown in Figure 2-4. The reversal region is smaller in the FL blade case than in the ML case, highlighting the reduction in the breakdown severity. The trailing edge pressure rise reduction in the FL blade was thus the reason for the 7% decrease in tip leakage loss.

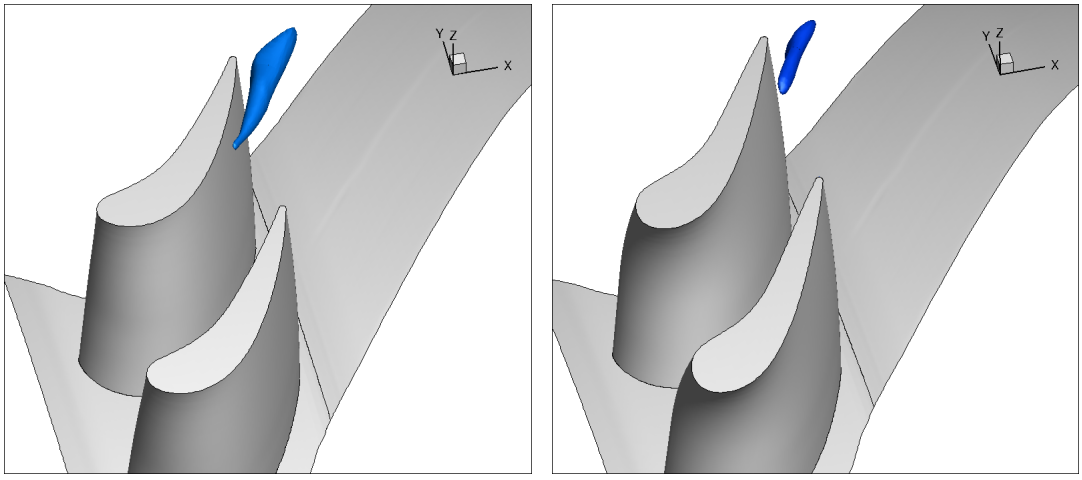

(a) (b)

Figure 2-4: Flow Reversal Regions in Tip Leakage Vortex Core (Shown by Blue Isosurfaces): a)ML blade, b)FL blade

2.5 Leakage Flow Analysis Metrics

2.5.1 Tip Leakage Loss Coefficient

The loss generated by the tip leakage flow is characterized by a tip loss coefficient $\xi_{tip} = \xi_{2\%clr} - \xi_{0\%clr}$, where a loss coefficient is as defined as in Equation 2.2.

$$\xi = \frac{T_{exit}\Delta s}{c_p(T_{t,inlet} - T_{t,exit})} \tag{2.2}$$

The tip loss coefficient is defined as the loss coefficient of a flow with a clearance

gap minus the loss coefficient of the same blading without a clearance gap modeled.

2.5.2 Tip Leakage Mass Flow

The magnitude and location of the leakage massflow exiting the gap is shown in Figure 2-5. Figure 2-5(a) shows the leakage massflow versus axial distance normalized according to Equation 2.3, is concentrated in the rear half of the blade. The quantity $\rho UA = \dot{m}_{main}$ is the axial massflow through the blade row.

$$\dot{m}_{normalized} = \frac{(\rho u)}{\rho UA} c\, g \tag{2.3}$$

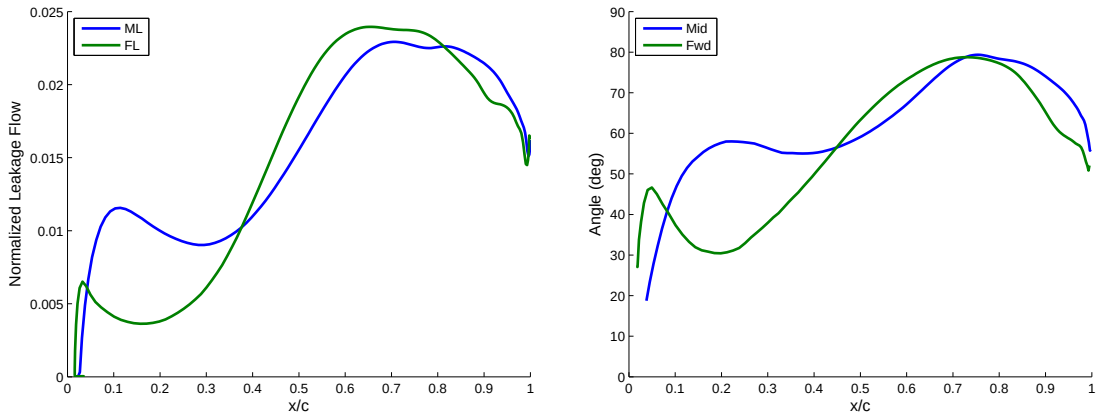

(a) (b)

Figure 2-5: Characterization of Tip Gap Leakage Flow Properties: a)Leakage Flow Distribution Versus Axial Position, b)Leakage Flow Angle Distribution (measured from streamwise direction) Versus Axial Position

Description of the gap exit flow also requires a leakage angle distribution, measured from the streamwise direction, as shown in Figure 2-5(b). The combination of the leakage flow distribution and the leakage angle distribution dictates the shear layer formation due to misalignment of the leakage flow and the passage flow velocities. This shear layer rolls up to form the vortex.

The gap coefficient of discharge describes how effectively the tip passes mass flow. An "ideal" leakage mass flow is calculated using the ratio of static to stagnation

pressure, with the static pressure taken to be that at gap exit. The ratio of actual massflow to ideal massflow for the tip gap is the coefficient of discharge. The axial distribution of C_d is shown for the ML and FL blades in Figure 2-6.

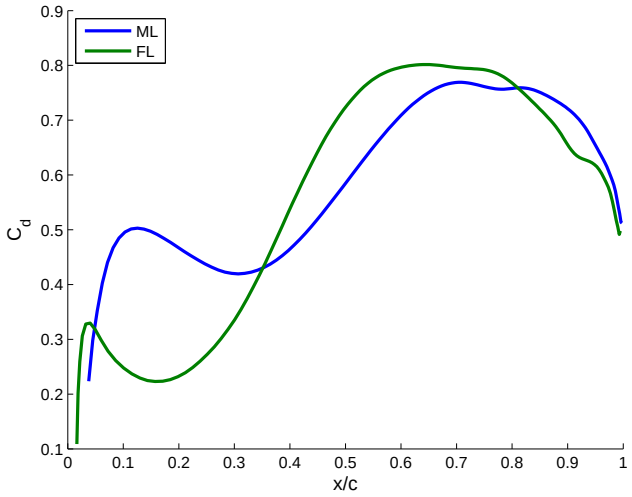

Figure 2-6: Characterization of Tip Gap Leakage Flow Properties: Gap Coefficient of Discharge Distribution

2.5.3 Tip Leakage Vortex State

The vortex evolution in the axial direction is important in setting the loss created by the tip leakage flow. An indication of vortex intensity is the swirl number, $S = v_\theta/u$. The average core axial velocity is u, and the swirl velocity v_θ is calculated using the vortex circulation and outer radius: $\Gamma = 2\pi r_e v_\theta$. Higher pre-breakdown swirl numbers create more mixed out loss [9]. An additional indicator of the vortex state is the centerline velocity ratio, defined as the minimum streamwise velocity in the vortex core, normalized by the magnitude of the freestream velocity downstream of the trailing edge.

The swirl number at the trailing edge changes between the ML and FL blades because of the differences in centerline velocity ratio. Figure 2-7 shows the deceleration in the core is less for the FL blade than for the ML blade (because the leakage vortex is subjected to a smaller pressure rise in the FL blade). For equal swirl velocity, the

lower axial velocity in the ML leakage vortex means a higher swirl number and thus more loss.

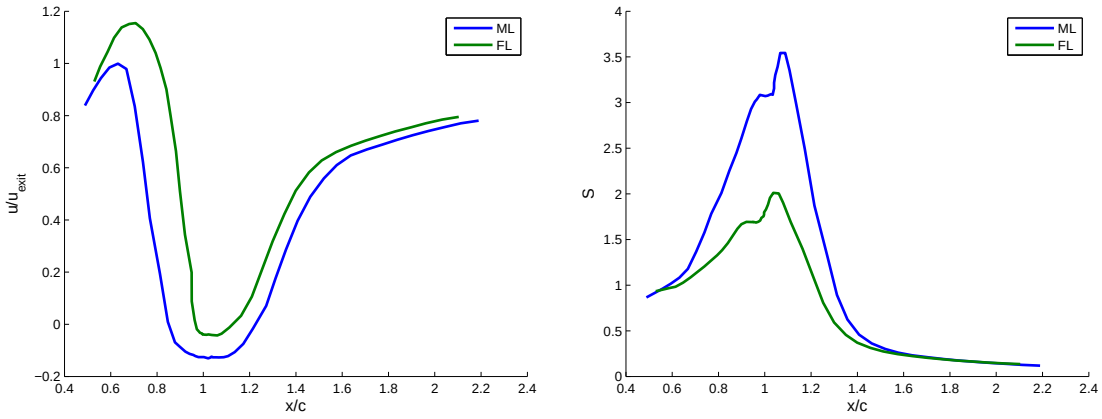

(a) (b)

Figure 2-7: Characterization of Vortex Properties Versus Axial Position: a)Core Centerline Velocity Ratio, b)Core Swirl Number

2.5.4 Tip Leakage Loss Generation

The axial distribution of loss generation can be used to highlight the regions that account for the majority of the tip loss. A peak in dissipation typically corresponds to the minimum streamwise core velocity axial location, where the difference between velocities in the core and freestream, Δu, is largest. Because mixing loss scales with $(\Delta u)^2$, this region contributes most heavily to the loss. Figure 2-8 shows the dissipation as a function of axial position (integrated over the upper 50% of the blade passage). The quantity given is the difference between the 2% and the 0% cases, with the dissipation for the 0% case subtracted from the 2% clearance case. The loss generated per unit axial distance, $^{d\xi}/_{d(x/c)}$, is calculated as in Equation 2.4. Figure 2-8 shows the peak due to vortex beakdown occurs at x/c = 1.1. The analysis does not include contributions from dissipation due to the boundary layer and the lower 50% of the blade passage.

$$\frac{d\xi}{d(x/c)} = \frac{T_{exit}c}{m_{main}} \int \rho \frac{ds}{dt} dA_{axialslice} \tag{2.4}$$

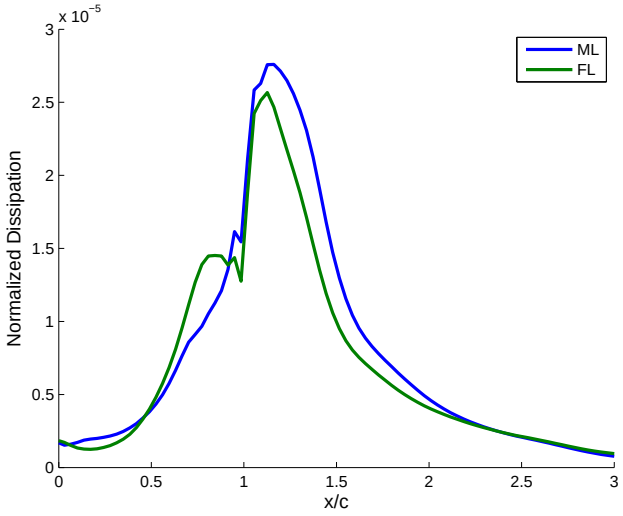

Figure 2-8: Characterization of Vortex Loss Generation Distribution (2% case - 0% case), $NormalizedDissipation = \frac{d\xi}{d(x/c)}/c_p \Delta T_t$

2.6 Turbulence Modeling Effects

Two turbulence models, Spalart Allmaras (SA) and $k-\omega$ Shear Stress Transport (SST), as well as two numerical codes, NUMECA FINE^{TM}/Turbo (FT) and Rolls-Royce HYDRA, have been used in this work. The main effect of turbulence model is on the turbulence production in the vortex core. One and two equation turbulence models tend to smear out the vortex core with more turbulence production [14], so vortex response to a pressure gradient is weaker than with a higher order model such as a full Reynolds Stress model [13].

Figure 2-9 shows the reduction of vortex core deceleration is more prominent in the FT calculation using the SA model. The flow field calculated using the SA model with the rotational correction responds more strongly to the external pressure, and the two SST model calculated flow responses are in between the two SA models implemented here. Changing the turbulence model impacts the absolute levels of the

vortex parameters, such as vortex centerline velocity ratio in the breakdown region (by ~ 0.2), but does not alter the tip loss reduction trends. The largest difference between tip loss coefficients in the four simulations described is 4.1%, as shown in Table 2.2.

The overall tip loss trends remain the same regardless of code or turbulence model. This was illustrated with a back-to-back study with a change in downstream diffusing duct geometry with the FT SA and FT SST models. An increase in duct area ratio of 65% caused tip loss coefficient increase of 3.6% with the FT SA model, and a 5.1% increase with the FT SST model. In summary, the results show that the turbulence model is not critical to assessing the impact of turbine environment on tip loss for the blades of interest.

Case	$\xi_{0\%clr}$	$\xi_{2\%clr}$	ξ_{tip}	% Change from FT SA
FT SA	0.0714	0.134	0.0631	
FT SST	0.0695	0.130	0.0605	-4.1
HYDRA SA	0.0668	0.131	0.0646	2.3

Table 2.2: Impact of Turbulence Model on Tip Loss Coefficient Behavior

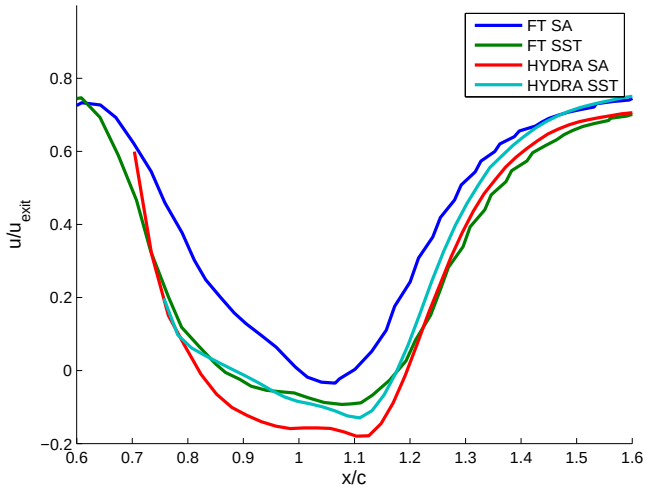

Figure 2-9: Effect of Turbulence Model and Code Implementation on Vortex Centerline: FINE^{TM}/Turbo SA, FINE^{TM}/Turbo SST, HYDRA SA, HYDRA SST

Chapter 3

Effect of Bowing Turbine Blade on Tip Leakage Vortex Mixing Losses

3.1 Introduction

The applicability of the tip leakage loss mechanism found by Huang has been examined for blade designs with three dimensional stacking changes, called bowing. Bowed blades are created by shifting constant two dimensional cross sections relative to one another in the tangential direction, similar to sliding a deck of cards, with positive bow referring to a radially concave suction surface of the blade. An example of a positively bowed blade is shown in Figure 3-1.

The blades described here were designed in a similar manner to the blades used in the study by Staubach et. al. [12], who calculated a 40% reduction in tip loss using both positive bow and axial sweep. The goal was to determine the magnitude and cause of changes in tip loss due to bowing. One possible cause is overall changes in the driving pressure difference across the tip, resulting in a smaller mismatch between gap exit velocity and main passage flow velocity. A second possible mechanism could involve the the behavior of the vortex in a pressure rise at the blade trailing edge described by Huang [9]. The effects of bowing a turbine blade on the tip loss coefficient were determined to address this question.

The effect of bowing on the tip loss behavior comes from changes in the radial

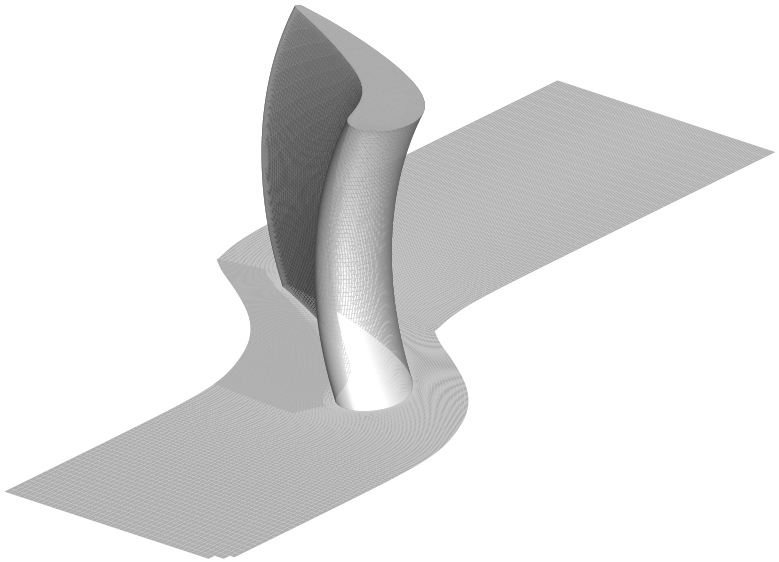

Figure 3-1: 115° Positive Bowed Blade Design

loading distribution. The concept is explained by Denton and Xu as a "frozen pressure field" [4]. Streamline curvature in the blade-to-blade plane is much higher than in the $r - \theta$ plane, so the blade-to-blade pressure gradient dominates. It is as if the blade geometry moves within a set of radial isobars while bowing, modifying the loading at the hub and tip. Positive bow unloads the hub and tip relative to mid span, while negative bow loads the hub and tip relative to mid span.

3.2 Computational Geometry

Linear cascades were used to simplify the analysis, with four bowing magnitudes examined: 65°, 90°, 115°, and 130°. A 90° blade is a straight blade, while a 115° blade means the tip has been shifted 25° past vertical. FINE^{TM}/Turbo was used with a grid of $\sim$ 3 million cells and y^+ of one. The computation inlet was 2 chords upstream of the leading edge and the outlet was 3 chords downstream of the trailing

edge.

3.3 Effect of Bow on Blade Passage Pressure Field

Calculations for no clearance cascades are shown in Figure 3-2, which illustrate the effect of bowing. The constant pressure lines are nearly radial despite the geometry shift in the circumferential direction. The figure also shows the change in radial loading; the 130° blade is higher loaded at midspan and less loaded near the tip compared to the straight blade.

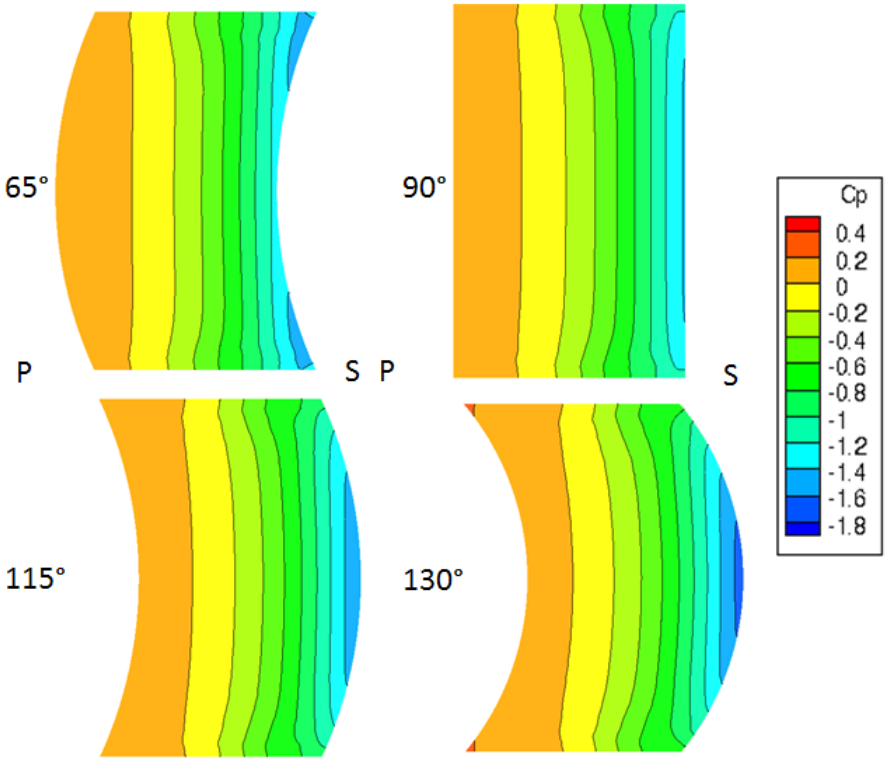

Figure 3-2: 115° Bowed Blade Static Pressure Contours at x/c = 0.5

Figure 3-3 illustrates the "frozen pressure field" concept in a different manner, using blade static pressure distributions at several spanwise locations for the 115° blade, no clearance case. The loading is less at radial locations closer to the tip compared to midspan. The pressures at 25% span match those at 75% because the blade is symmetric about the midspan. The impact of bowing is concentrated in the

first 70% axial chord of the blade.

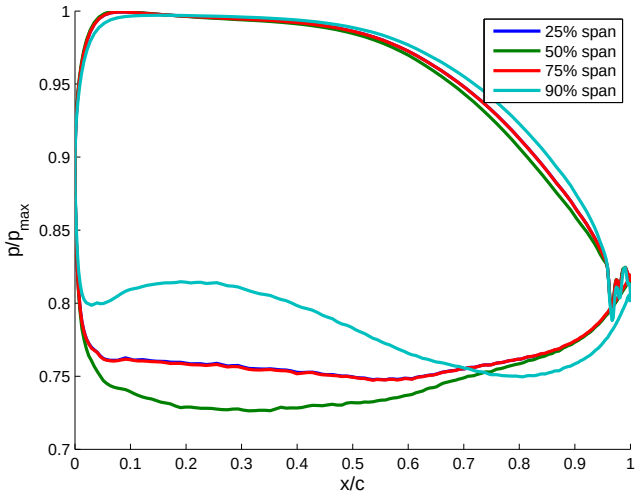

Figure 3-3: Radial Loading Variation due to Bow: 115° Blade, No Clearance

The pressure profiles in Figure 3-4 at 90% span show the effect of bowing on near-tip loading. The near-tip loading decreases monotonically as the blade angle increases from 65° to 130°. This result will be shown to have important implications for loss.

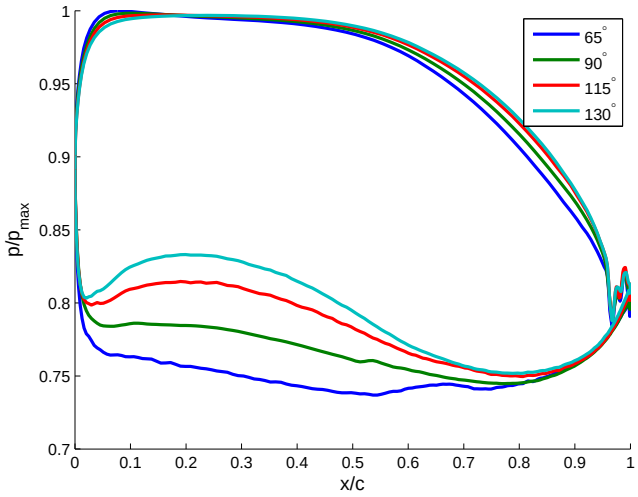

Figure 3-4: Tip Loading Variation due to Bow: 90% Span, No Clearance

3.4 Results

3.4.1 Tip Leakage Loss

The computations show that positive bow has a beneficial effect on the tip loss. In the most extreme case of the 130° blade, the tip loss coefficient is reduced by 20% compared to the baseline straight blade, as in Table 3.1. There is a reduction in tip loading due to bowing which reduces the gap exit velocities, and thus the difference between tip leakage flow and main passage flow velocities ($|\Delta\vec{v}|$). Since mixing loss scales with $(|\Delta\vec{v}|)^2$, and positive bow reduces this value, the leakage loss decreases.

Bow Angle	$\xi_{0\%clr}$	$\xi_{2\%clr}$	ξ_{tip}	% Change from 90°
65	0.0401	0.0734	0.0332	2.3
90	0.0368	0.0693	0.0325	0.0
115	0.0409	0.0707	0.0297	-8.4
130	0.0477	0.0737	0.0260	-20.0

Table 3.1: Influence of Bowing on Tip Loss Coefficient Behavior

3.4.2 Tip Leakage Massflow

Table 3.2 gives the changes in normalized tip leakage flow relative to the straight blade for different bowing magnitudes. There is an increase in leakage flow with positive bow. There are several impacts on the leakage flow magnitude, including tip loading and the behavior of the velocity field inside the gap.

Bow Angle	$\dot{m}_{main}$ (kg/s)	$\dot{m}_{tip}$ (kg/s)	Normalized $\dot{m}_{tip}$	% Change from 90°
65	0.115	0.0057	0.0498	-3.78
90	0.115	0.0059	0.0518	0.0
115	0.117	0.0061	0.0526	1.61
130	0.116	0.0062	0.0532	2.85

Table 3.2: Influence of Bowing on Leakage Flow Behavior

The tip massflow increases as the blade is positively bowed, which is not expected given the decrease in near-tip blade loading. The reason is that the discharge coef-

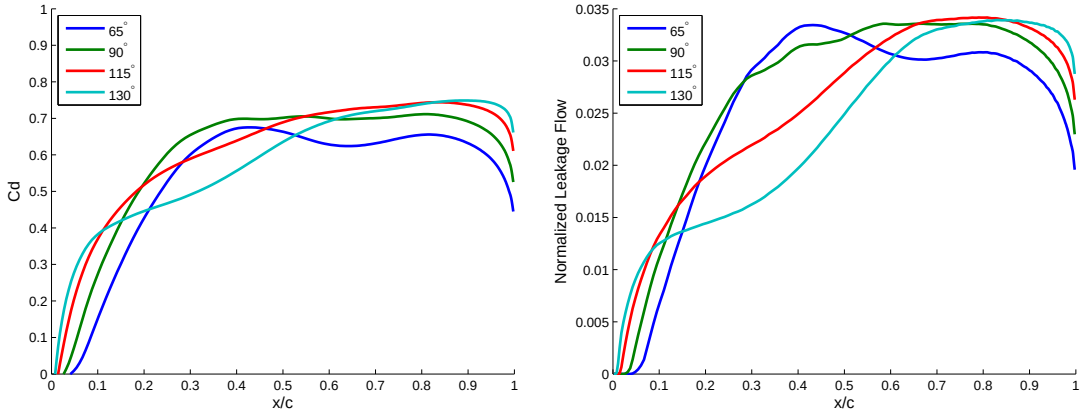

(a) (b)

Figure 3-5: Influence of Bowing on Tip Leakage Flow: a)C_d Distribution, b)Leakage Flow Distribution

ficient for the tip flow, C_d, increases as the blade is bowed. This is shown in Figure 3-5(a), which gives the axial distribution of C_d. The mean C_d increases from 0.57 for the 65° blade to 0.65 for the 113° blade.

The physical basis for the C_d behavior can be seen from the velocity field at the corner of the gap entrance in Figure 3-6. A separation bubble forms with a vena contracta in the gap flow due to the sharp corner on the pressure side of the blade. The influence of the separation bubble increases as the size of the low pressure region at the gap corner increases. This bubble decreases in size with positive bow; the bubble for the 130° blade in Figure 3-6 is smaller than the bubble for the 65° blade. A smaller separation allows more massflow with corresponding higher C_d. The result is a 3% increase in normalized leakage mass flow for the 130° blade relative to the straight blade, despite the reduction in tip loading.

3.4.3 Tip Leakage Vortex State

The effects of loading changes due to bow can be seen in the vortex parameters in Figure 3-7. The core velocity ratio minimum increases with increasing bow and the swirl number of the tip leakage vortex reduces. Increasing bow reduces the vortex

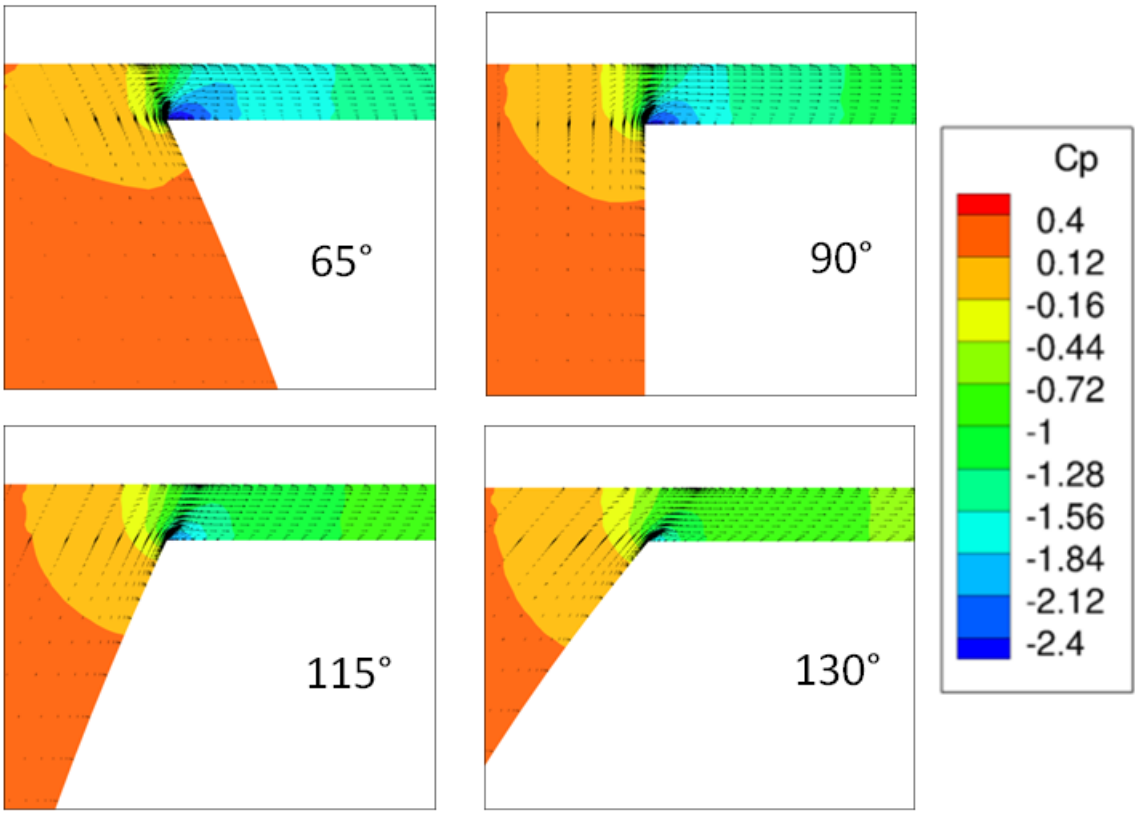

Figure 3-6: Gap Entrance Flow Field Characteristics at x/c = 0.25 (Pressure Side Corner) for Different Bowing, with Overlaid In-Plane Velocity Vectors

strength, which creates less leakage loss from mixing with the freestream.

Figure 3-8 presents the vortex centerline static and stagnation pressure coefficients as a function of axial position. The differences in the static pressure rise undergone by the vortex are small (Figure 3-8(a)). The pressure in the core is sensitive to the external pressure gradient because the core is swirling, so if no changes are evident in core pressure response, the external pressure rise between the cases should be similar. The 65° blade, however, has a lower stagnation pressure at the gap exit than the 130° blade due to increased mixing within the gap from the larger separation bubble, as given in Figure 3-8(b). For similar pressure gradients a reduced stagnation pressure in the core results in an increased deceleration, and this is the situation in the negatively bowed blade vortex core. The result is lower centerline velocity, higher swirl number, and more loss.

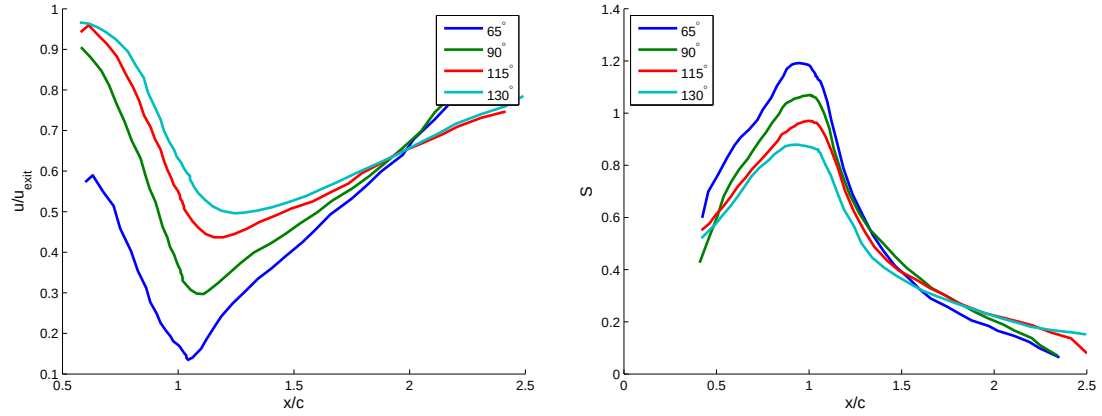

(a) (b)

Figure 3-7: Influence of Bowing on Vortex Core: a)Centerline Velocity Ratio, b)Swirl Number

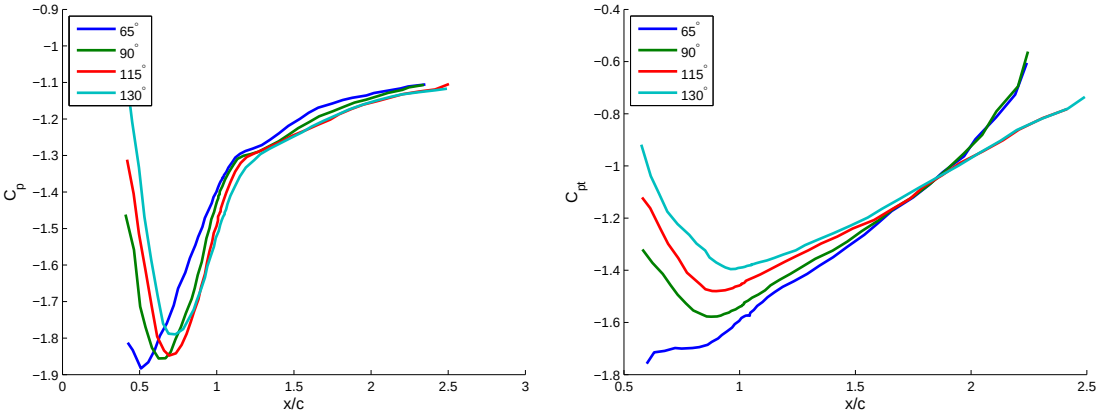

(a) (b)

Figure 3-8: Influence of Bowing on Vortex Core: a)Centerline Static Pressure, b)Centerline Stagnation Pressure, $C_p = \frac{p-p_{in}}{q_{in}}$, $C_{pt} = \frac{p_t-p_{t,in}}{q_{in}}$

3.4.4 Tip Leakage Loss Mechanisms

The changes in tip leakage loss can be attributed to the differences in overall loading at the tip. Arguments for this can be made using a control volume analysis outlined by Denton [3]. In this method, the flow is mixed out at constant pressure, equal to the suction side pressure at the point of gap exit, to determine the leakage loss.

The expression for loss is Equation 3.1, evaluated at the tip gap exit during CFD post-processing to produce the results.

$$Tds_{gen} = \int \frac{\rho V_{leak} sin(\epsilon)}{m_{main}} \left(\frac{1}{2} \left[V_{leak}^2 + V_{ss}^2 - 2V_{ss}V_{leak}cos(\epsilon) \right] + c_p T \int_T^{T_{inj}} -\frac{1}{\tau} d\tau \right) gdx \tag{3.1}$$

The results of the control volume loss analysis using Equation 3.1 are shown in Figure 3-9, which illustrates the distribution of contribution of the tip leakage flow to the mixing loss versus axial location. The loss generation is concentrated towards the trailing edge, because the leakage flow is also concentrated towards the aft portion of the tip gap.

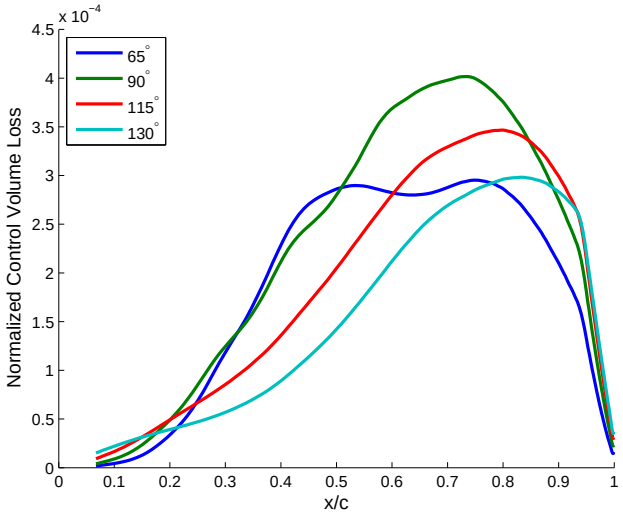

Figure 3-9: Influence of Bowing on Loss Distribution for Leakage Flow Mixed Out at Constant Pressure, $Normalized\ CVloss = {}^{T_e ds}/_{c_p \Delta T_t}$

Table 3.1 shows the total control volume loss, integrated under the curves of Figure 3-9. Comparison of Tables 3.3 and 3.1 show the control volume analysis yields tip loss changes for the 90° and 130° bowed blades in accord with the CFD predicted tip loss coefficient changes. However, the control volume analysis does not capture the effect of changing pressure during leakage flow mixing as shown by Huang [9]. If the control volume analysis captures the loss benefit due to blade bowing, it can be concluded

that the changes in tip loss coefficient are dominated by overall tip loading. This analysis is supported by the vortex state analysis, because the changes seen were due to a similar pressure rise acting on vortex cores with different stagnation pressures, rather than due to variation in trailing edge pressure rise (as in the ML and FL blade comparisons).

Bow Angle	ξ_{CV}	% Change from 90°
65	0.0305	-20.29
90	0.0383	0.0
115	0.0344	-10.12
130	0.0295	-22.90

Table 3.3: Influence of Bowing on Integrated Control Volume Tip Loss Coefficients

3.5 Conclusions

The effect of blade bowing on tip leakage loss was assessed using three-dimensional calculations for a turbine cascade. The radial distribution of blade loadings agreed with the "frozen pressure field" concept proposed by Denton and Xu, giving nearly radial isobars when viewed in the $r-\theta$ plane [4]. There were larger total gap leakage massflows for the positively bowed blades despite reduced tip loading because of smaller separation bubbles at the corner of the gap entrance, which led to larger coefficients of discharge for increased positive bowing. The tip loss benefit of 20% for the 130° blade, compared to the straight blade, is due to the overall reduction in loading. A control volume analysis of the gap exit flow also gave this result, indicating the overall tip loading is the dominant effect on tip leakage loss.

Chapter 4

Effect of Transition Duct Geometry on Tip Leakage Vortex Mixing Losses

4.1 Introduction

Turbine blades in gas turbine engines do not operate in isolation. For a single stage high pressure turbine, for example, the flow enters a downstream diffusing transition duct before reaching the low pressure turbine. Computations were thus performed to assess the impact of transition duct design on the tip leakage loss.

4.2 Design of Transition Ducts

The diffusing transition ducts were designed to cover a parameter space defined by non-dimensional wall length, area ratio, and inner and outer wall angles. The two most influential of these are area ratio (AR), and non-dimensional wall length ($\bar{L}/\Delta R_d$). For diffusers, Sovran and Klomp defined a c_p^{**} curve as the locus of designs that have the highest pressure recovery for a given area ratio, and a c_p^* curve as the locus of designs that give maximum pressure recovery for a given non-dimensional length [11]. Figure 4-1 shows the c_p^* and c_p^{**} curves in AR-1 versus $\bar{L}/\Delta R_d$ space.

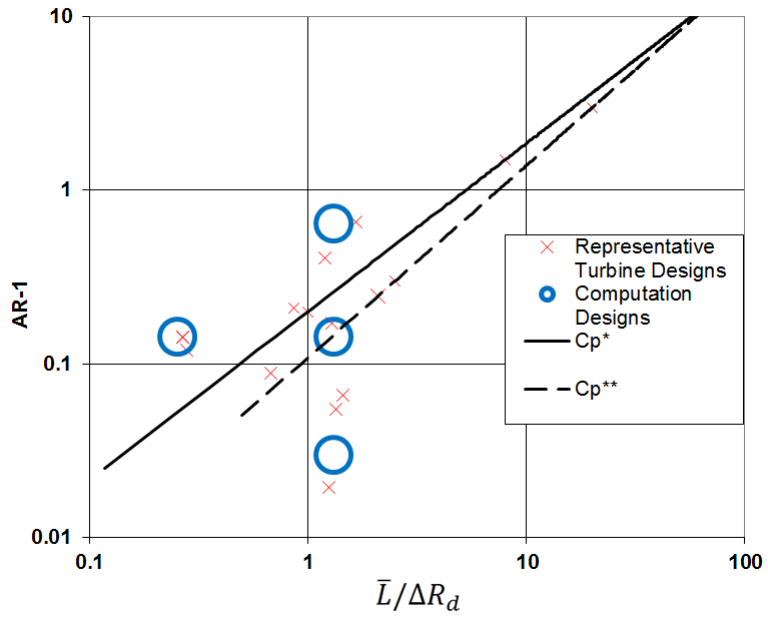

Figure 4-1: Transition Duct Design Space (AreaRatio - 1 vs. Non-dimensional Duct Length): With c_p^* and c_p^{**} curves from Sovran and Klomp [11]

The figure also shows four circles representing the cases examined. These cover a representative design space for turbine transition ducts.

The four designs corresponding to the circles in Figure 4-1 are shown in Figure 4-2, with Transition Duct 1 corresponding to the point on the c_p^{**} curve. A straight duct, called Transition Duct 0, was also modeled to serve as a baseline.

The outer wall angles were held constant for this set of calculations at 20°, with the idea of keeping local effects due to the upper duct corner the same for all cases. The inner wall angle and the wall lengths were not constant, and are specified by the desired AR and $\bar{L}/\Delta R_d$.

4.3 Computational Details

NUMECA FINE^{TM}/Turbo with the ML blade geometry was used for this set of calculations. A grid density of ~3 million cells was used and the SA turbulence model was implemented with a y^+ of about 1.

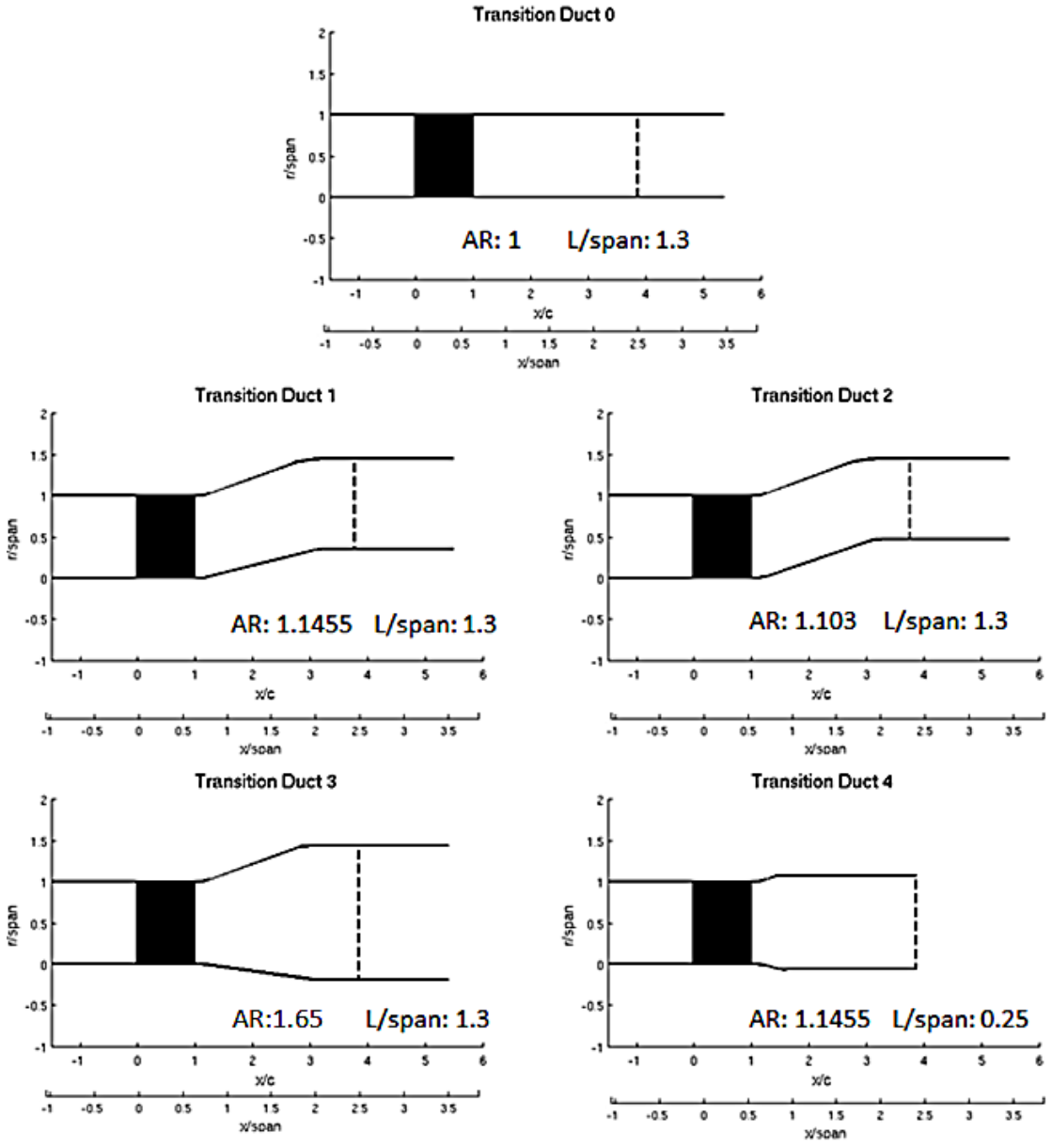

Figure 4-2: Meridional View of Transition Duct Designs: Blade Represented by Solid Rectangle, Evaluation Location for ξ Represented by Dashed Line

The computational domain extended 1.5 chords upstream of the blade leading edge and 1 diffuser exit span downstream of each diffuser exit. The former was done to decouple the inlet conditions from the upstream influence of the blade, and the latter was done to allow the flow to mix out before being subjected to the static pressure equilibrium boundary condition. The exit pressure at the duct exit hub location was set to ensure the work done by each blade matched within ±0.5% relative to the work done in the Transition Duct 0 case.

The loss evaluation was done at different axial locations in each of the four ducts. The evaluation location was chosen so that the mean radius flow path distance was constant to provide equal opportunity for the leakage flow to mix with the freestream. The corners of the hub and casing at the start and end of the transition duct were designed with a radius of curvature corresponding to 20% of the hydraulic diameter (D_h) of the annular duct to avoid separation [5]. The corner of the transition duct is located 0.1 axial chords downstream of the blade trailing edge according to standard design practice [5].

4.4 Results

4.4.1 Tip Leakage Loss

Table 4.1 presents the tip loss coefficients for all ducts. The increases in area ratio caused small increases in tip loss, with the most extreme AR of 1.65 causing a 3.6% increase in tip loss coefficient compared to the baseline. The loss increase is due to further deceleration of the core, which strengthens the vortex breakdown.

Duct	$\xi_{0\%clr}$	$\xi_{2\%clr}$	ξ_{tip}	% Change from 90°
0	0.0714	0.134	0.0631	0.0
1	0.0703	0.135	0.0693	2.39
2	0.0723	0.136	0.0635	0.76
3	0.0715	0.137	0.0654	3.64
4	0.0684	0.131	0.0621	-1.56

Table 4.1: Transition Duct Tip Loss Coefficient Behavior

4.4.2 Tip Leakage Massflow

The blade loading was altered little between duct designs, so the variation in tip leakage flow is negligible. The results are given in Table 4.2 for completeness.

Duct	$\dot{m}_{main}$ (kg/s)	$\dot{m}_{tip}$ (kg/s)	Normalized $\dot{m}_{tip}$
0	0.314	0.0232	0.0739
1	0.313	0.0232	0.0741
2	0.313	0.0232	0.0741
3	0.314	0.0232	0.0740
4	0.314	0.0233	0.0742

Table 4.2: Influence of Transition Duct Geometry on Leakage Mass Flow

4.4.3 Influence of Duct Design on Axial Pressure Rise and Blade Loading

Figure 4-3 shows the circumferentially averaged pressure rise as a function of axial position experienced by the mean flow in the duct downstream of the blade. The largest pressure rises correspond to ducts 3 and 4 which are the most aggressive.

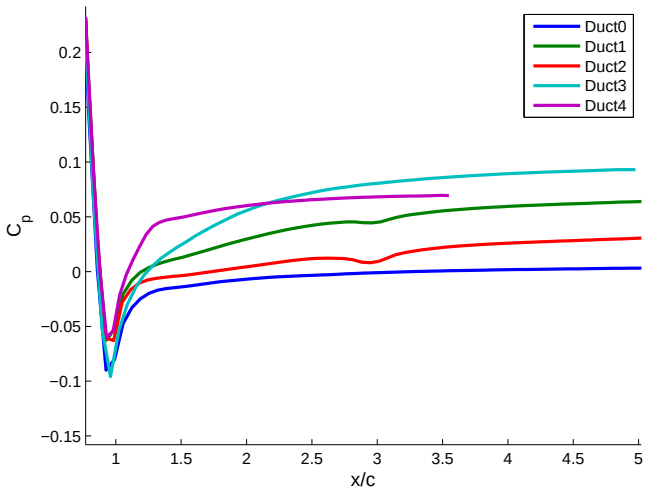

Figure 4-3: Axial Distribution of Average Static Pressure in Duct, 2% Clearance, $C_p = \frac{p - p_{x/c=1}}{q_{x/c=1}}$

The duct corners are located 0.1 chords downstream of the blade trailing edge, thus it can be expected that they will have some upstream influence on the blade exit flow. Figure 4-4 shows radial distributions of static pressure at blade exit, illustrating that the duct corner on the upper wall causes a local decrease in static pressure. This is most clearly shown in the difference between ducts 0 and 2 because they have similar area ratios. A similar argument can be made for the bottom corner, except the sign of the local pressure change varies between duct designs because some ducts have positive wall angles while others have negative angles.

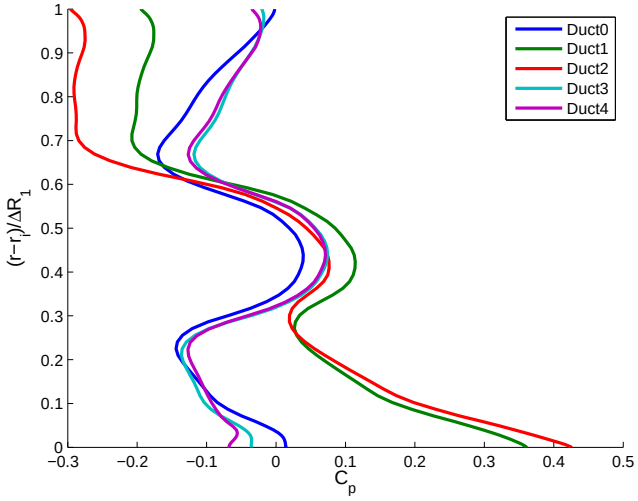

Figure 4-4: Radial Distribution of Circumferentially Averaged Pressure at Blade Exit, 0% Clearance, $C_p = \frac{p - p_{x/c=1}}{q_{x/c=1}}$

Despite ducts 1-4 having the same 20° outer wall angle, there are differences in the near-tip static pressures shown in Figure 4-4. This is caused by a variation in the strength of the upstream influence of the downstream diffuser geometry. Duct 2 has the smallest AR so the depression in static pressure in the upper half of the channel is the largest. Duct 1 has a larger AR, so the pressure rise downstream created by the diffuser influences the pressure field at blade exit and raises the pressure in the upper 30% of the duct relative to that of Duct 2. The same occurs for Ducts 3 and 4 in increasing magnitudes.

The result of the variation in upstream influence due to duct geometry is that the

trailing edge blade loading profiles near the tip are altered slightly as shown in Figure 4-5, although the net effect of this loading change is small. There are no discernible changes in leakage flow, and the vortex properties on the blade are not affected as will be shown in the subsequent sections.

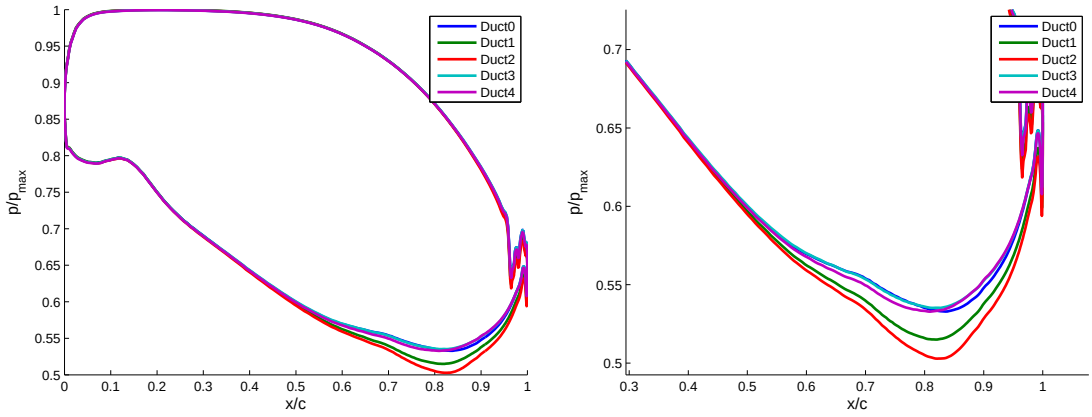

(a) (b)

Figure 4-5: Upstream Influence of Transition Duct on Blade Loading Profile at 90% Span, 0% Clearance

4.4.4 Tip Leakage Vortex State

The centerline velocity ratio and dissipation data are nearly indistinguishable between duct geometry cases as shown in Figure 4-6 and Figure 4-7. However, if the breakdown regions are examined, small differences are present which agree with the prior finding that dissipation is larger in vortex cores with lower minimum core velocities. Ducts with larger pressure rise, such as Duct 3, have lower minimum velocities in the vortex core compared to Duct 1. In addition, this means lower swirl numbers for Ducts 1 and 2 as shown in Figure 4-8. The lower minimum velocity ducts in Figure 4-6 correspond to the curves with higher dissipation peaks in Figure 4-7. However, the effect of the dissipation changes is 3.6% in tip loss coefficient for the most extreme duct despite the 65% change in AR.

We emphasize that the effect of the transition duct on the vortex properties is

small when compared to changes seen by Huang due to blade geometry [9]. The largest changes for the duct cases are on the order of 0.05 for the velocity ratio and 12.5% for the dissipation, compared to changes of 0.15 velocity ratio and 30% in dissipation due to blade loading distribution changes.

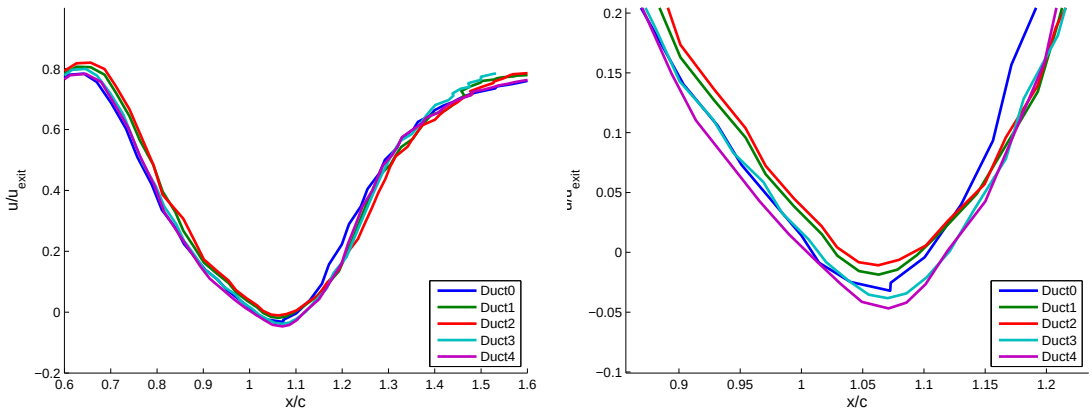

(a) (b)

Figure 4-6: Vortex Velocity Ratio Changes Due to Transition Duct Design

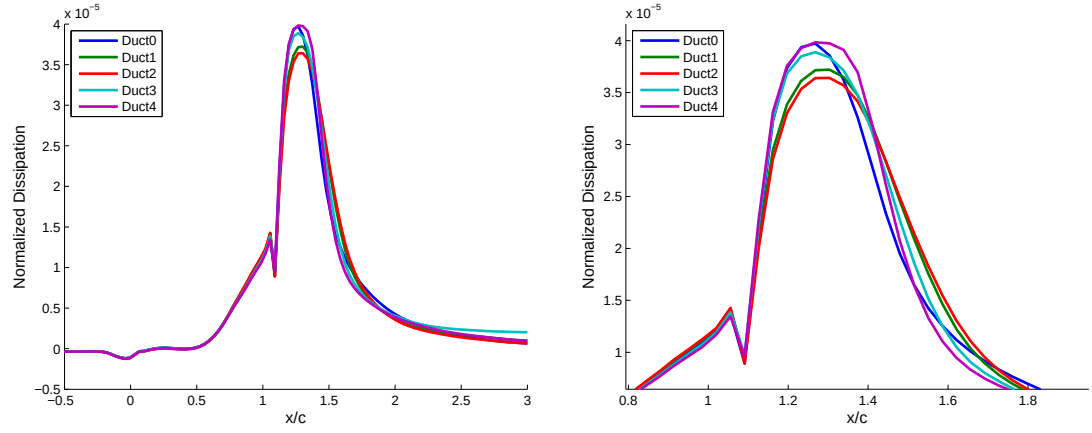

(a) (b)

Figure 4-7: Vortex Loss Generation (2% case - 0% case) Changes Due to Transition Duct Design, $NormalizedDissipation = \frac{d\xi}{d(x/c)}/c_p \Delta T_t$

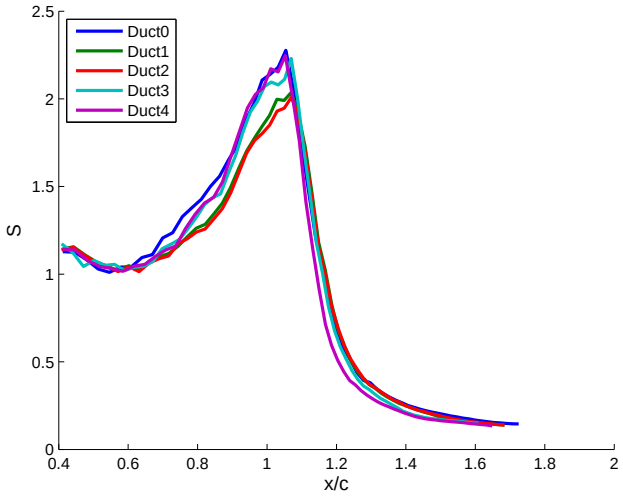

Figure 4-8: Vortex Swirl Number Changes Due to Transition Duct Design

4.4.5 Tip Leakage Loss Mechanisms

The reasons for the small effect of duct geometry effect are twofold. First, the pressure changes created by the duct diffusion occur over a larger distance (2 axial chords), than the pressure changes on the blade surface (0.2 axial chords). A given pressure rise difference between duct designs corresponds to an order of magnitude smaller change in pressure gradient than in the blade tip design variation study. The blade tip vortex properties are thus similar for the various downstream diffusing duct designs and, correspondingly, the tip loss coefficients are similar.

Further, the regime in which the duct pressure gradient acts on the vortex is one of low sensitivity for changes in pressure rise. The vortex mixes quickly downstream of the trailing edge and by x/c = 1.4 the swirl number has fallen to 0.2 and the velocity ratio has risen to 0.7. The duct extends over the range x/c = 1 to x/c = 3, so for more than 75% of the duct the pressure rise acts on a weakly swirling vortex with a small velocity defect.

The difference in sensitivity of (axisymmetric) vortices subjected to a pressure rise are shown in Figure 4-9, which shows the increases in mixing loss as a contour plot in a core velocity ratio and swirl number plane. This figure enables a comparison

of vortex regimes at different axial locations [9]. The regime that corresponds to the pre-breakdown tip leakage vortex in the range of x/c = 0.6-1.1 is SN = 0.8-1.2 and VR = 0.0-0.3 near the letter B. This region, which exhibits strong sensitivity to pressure rise, is the regime on which the tip loading changes act. Region A shows lower sensitivity to pressure rise than region B, and is characterized by SN = 0.0-0.3 and VR = 0.6-0.8. This is why larger changes in loss are created when the loading is changed from aft to forward style (16%). The difference in vortex state is one reason why the vortex response is small relative to the vortex response based on tip loading distribution changes.

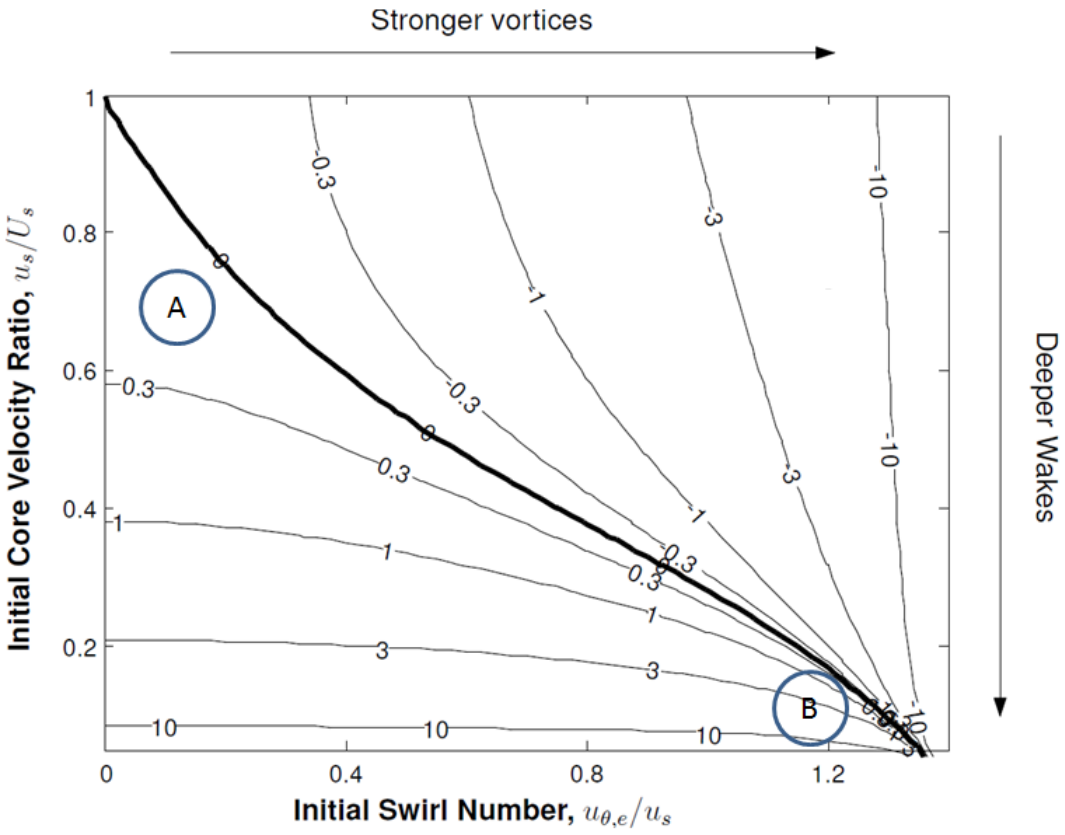

Figure 4-9: Swirling Flow Mixing Loss: Letter A:Vortex Regime in Transition Duct (Weakly Swirling), Letter B:Vortex Regime at x/c = 1 (Strongly Swirling) [9]

4.4.6 Combined Blade Loading and Transition Duct Effects

A set of computations was done to assess the interaction of effects from combined blade tip geometry changes and duct geometry changes. The tip loss coefficients are compared for four cases using the ML and FL blades and ducts 0 and 3 in Table 4.3. The table shows a reduced tip loss increase between ducts 0 and 3 with the FL blade (0.9%) compared to the tip loss increase with the ML blade (3.6%).

	Duct 0 ξ_{tip}	Duct 3 ξ_{tip}	% Change from Duct 0
ML ξ_{tip}	0.0631	0.0654	3.6
FL ξ_{tip}	0.0578	0.0583	0.9
% Change from ML	-8.4	-10.9	

Table 4.3: Interaction Effect of Duct Geometry and Blade Geometry on Tip Loss

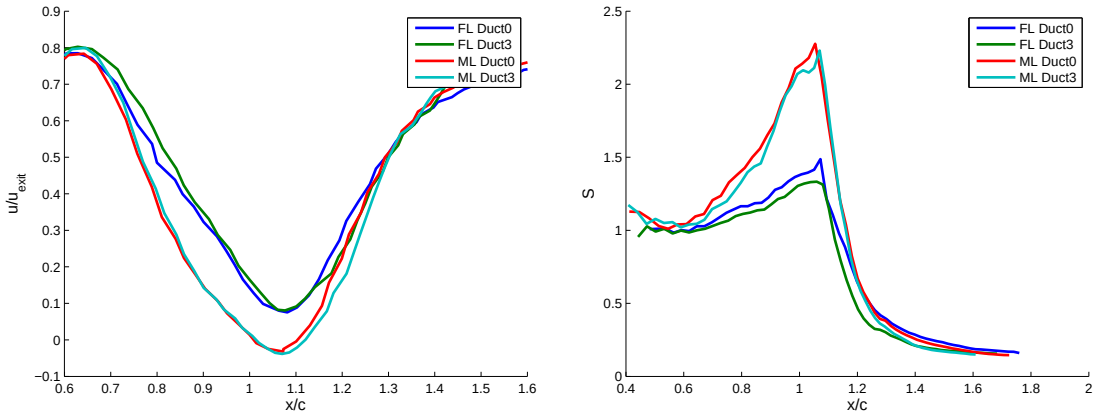

(a) (b)

Figure 4-10: Interaction of Duct Geometry and Blade Geometry Effects on Vortex State: a)Vortex Centerline Velocity Ratio, b)Vortex Swirl Number

The reason for the change in loss behavior for the FL blade is due to further reduction of vortex sensitivity in the duct compared to the ML blade. Figure 4-10 shows peak swirl number is reduced in the FL blade cases, and the deceleration of the streamwise velocity is not as severe, thus the tip leakage vortex is further desensitized to downstream pressure changes compared to the ML blade. This agrees with the tip loss coefficient results in Table 4.3. A second result is that the tip loss benefit

of forward loading the blade is 10.9% in the AR 1.65 duct, which is larger than the 8.4% for the same blade tip geometry change in the straight duct.

4.5 Conclusions

The impact of the downstream diffusing transition duct geometry on tip loss was assessed. Parameterization of the duct design was based on work by Sovran and Klomp, which showed the diffusing duct area ratio and non-dimensional length were the dominant parameters [11]. Five ducts, including one straight duct, were assessed to cover the range of existing transition duct designs. The tip loss coefficient increased 3.6% relative to the straight duct for an AR of 1.65. The changes in loss coefficient were smaller than those seen due to blade tip geometry changes because: i) the duct pressure rise acts on a vortex that is in an insensitive regime with both reduced swirl and higher core velocity ratio, and ii) the duct geometry creates pressure gradient changes that are an order of magnitude less than pressure gradient changes that result from forward loading the blade.

Chapter 5

Time Average Effects of Unsteady Upstream Vane Influence on Tip Leakage Vortex Mixing Losses

5.1 Introduction

Real turbomachines operate in an unsteady environment, and an important question is the impact of unsteadiness on tip leakage loss. To assess this, unsteady simulations of a vane-blade (stage) configuration have been conducted. The aim of the simulations was to address how turbine tip loss mechanisms are affected by unsteadiness due to an upstream nozzle guide vane, and a specific item of interest was how the vortex breakdown mechanism described by Huang was affected.

The discussion in this chapter concerns time averaged results, Chapter 6 will address the unsteady effects of the vane-blade configuration. The specific questions to be addressed are:

- What is the time average impact of unsteadiness on the overall loss coefficient?
- What is the time average impact of unsteadiness on the tip loss coefficient?
- Does the loss mechanism discovered by Huang hold in the vane-blade configu-

ration for unsteady flow?

- What is the time average impact of unsteadiness on the vortex properties and dissipation due to leakage flow?

5.2 Computational Details

The Rolls-Royce proprietary CFD code, HYDRA, was used for all unsteady calculations. The upstream vane and blade were first modeled in a steady manner, with mixing plane calculations performed on the ML and FL blades for 0% and 2% tip clearance cases. The steady simulations were then used as the starting point for a matching set of unsteady phase lag boundary condition cases.

To assess convergence, unsteady probes, which record the flow data at a given point in space, were inserted into the computational domain. There were 5 on the trailing edge of the vane, 5 on the leading edge of the blade, and 2 at midspan of the sliding interface between vane and blade. In addition, the cases with tip clearance had 5 probes inside the gap evenly spaced in the axial direction, and 5 probes inside the volume occupied by the tip leakage vortex. The probes were monitored to ensure periodic behavior was observed. The quantitative assessment of convergence was done using a fast Fourier transform to characterize the frequency content of these pressure probes. Figure 5-1 shows the amplitude of the unsteady pressure signal at the vane passing frequency for a probe in the blade relative frame versus computation time. The simulation covered 108 vane passings, and over the last ½ revolution the amplitude varies less than 0.1% per vane passing relative to the unsteady pressure amplitude corresponding to the last simulated vane passing.

Two sets of cases were run. The first set used the design airfoil counts of 36 vanes and 58 blades. This meant that the smallest periodic sector of the stage was half of the blades (18 vanes and 29 blades), so phase lagging was used to reduce the computational requirements. The grid used for these calculations is shown in Figure 5-2. The second set used modified airfoil counts of 29 vanes and 58 blades. This enabled a calculation to be run with a periodic sector that included one vane and two

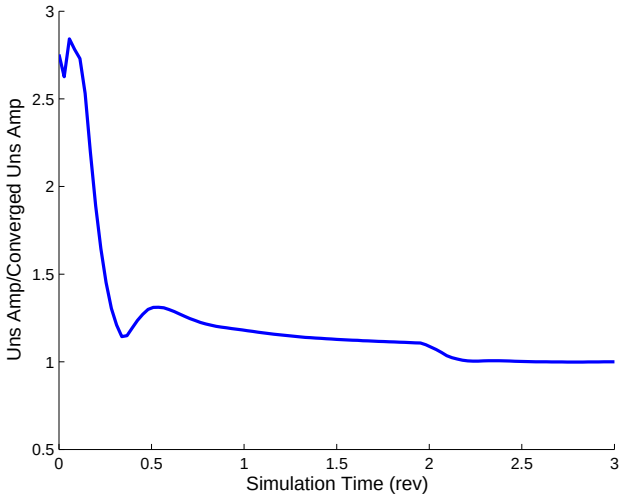

Figure 5-1: Analysis of Unsteady Probe Pressure Data Shows Convergence: Normalized Vane Frequency Response Amplitude versus Simulation Time

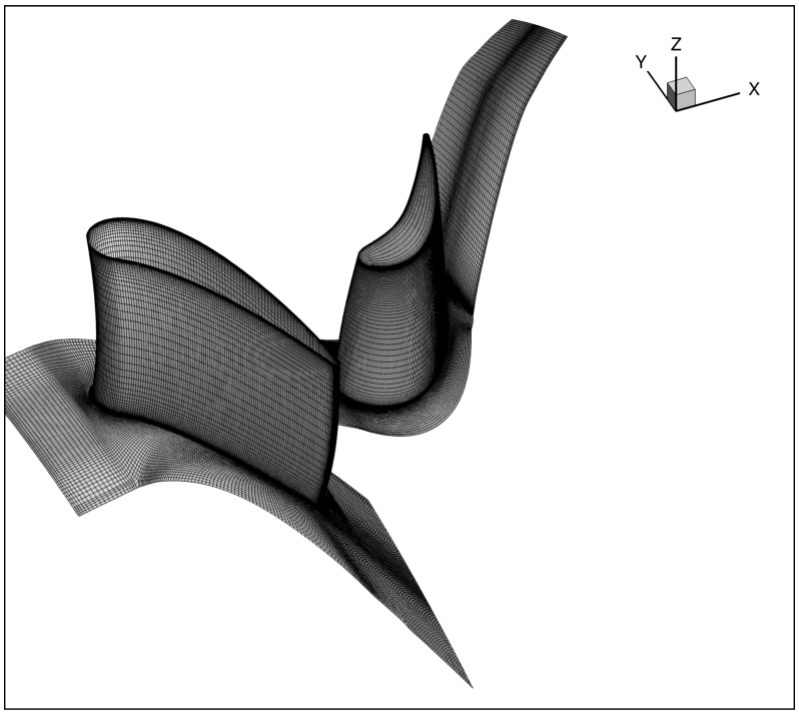

Figure 5-2: Sample Grid for Phase Lag Computations

blades. A sliding plane calculation was used for this second configuration, because the periodic sector was small enough to not require phase lagging. The discussion of data in this chapter is mainly from the calculations with the original airfoil counts.

The modified vane count cases, which had larger unsteady variations due to the 2 to 1 blade to vane ratio, will be discussed in Section 5.5.

5.2.1 Evaluation of the Unsteady Flow in the Tip Vortex

There were 116 time steps per vane passing period in the calculation. To enable analysis of this large data volume, each flow file was interpolated to the streamwise grid shown in Figure 5-3(a). This allowed calculation of streamwise velocity and vorticity on slices perpendicular to the vortex core path. The streamwise grid has 90% fewer grid points than the two blade passage mesh in order to reduce data requirements by eliminating unwanted information. To reduce the data further, volume average quantities were calculated for the subzone shown in green of Figure 5-3(b), referred to as the *breakdown control volume*. The breakdown volume extends from axial location x/c = 0.7 to x/c = 1.2 and thus includes the region in which the majority of the loss is generated.

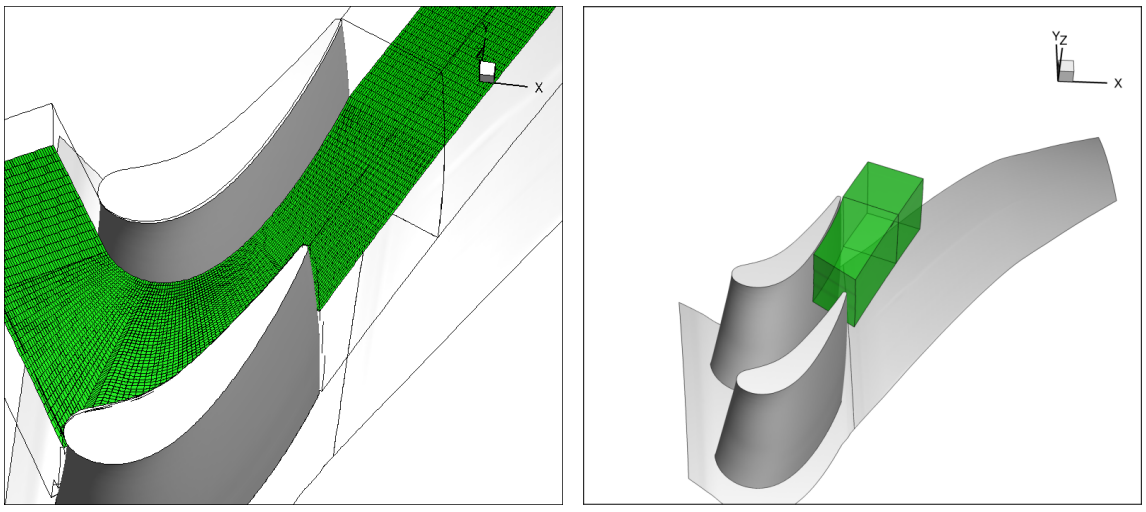

(a) (b)

Figure 5-3: Vortex Analysis Flow Field Domains: a)Radial Slice of Streamwise Grid, b)Vortex Breakdown Analysis Control Volume

5.3 Effect of Unsteadiness on Time Average Loss Coefficient

Table 5.1 shows that the time average overall loss coefficient increases by $4-5\%$ compared to the steady loss coefficient for the stage.

	ML 0%	ML 2%	FL 0%	FL 2%
Steady ξ	0.0695	0.143	0.0729	0.141
Unsteady ξ	0.0732	0.149	0.0764	0.147
% Difference	5.2	4.2	4.8	4.0

Table 5.1: Impact of Unsteadiness on Time Average Stage Loss Coefficient

Figure 5-4 shows radial profiles of mass average non-dimensional entropy at two axial locations, one upstream of the blade and one downstream of the blade, for the no clearance case. There is an increase in entropy at the hub and tip and a reduction in entropy near midspan for the unsteady time averaged solution. The source of the entropy increase is concentrated in the hub and tip passage vortices.

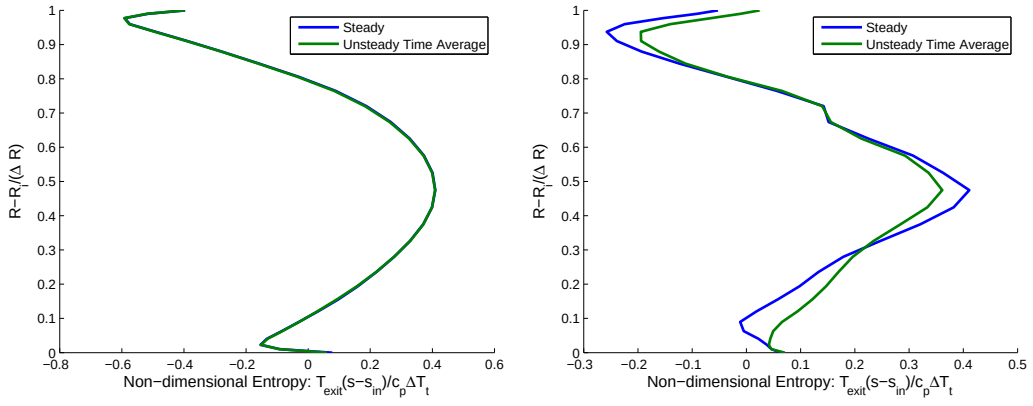

Figure 5-4: Radial Profiles of Mass Average Entropy Profiles, Circumferentially Averaged, No Clearance ML Blade: a)x/c = -0.25, b)x/c = 1.5

5.3.1 Effect of Unsteadiness on Time Average Tip Loss Coefficient

The effect of unsteadiness on time average tip loss is shown in Table 5.2. There is a roughly 3% increase in tip loss due to unsteadiness. The time average tip loss reduction of the FL blade in an unsteady vane-blade configuration is 7.7% compared to the ML blade, roughly the same as in steady flow (7.5%). To understand the tip loss coefficient behavior, the details of the tip leakage flow are examined in the following sections.

	ML	FL	% Difference from ML
Steady ξ_{tip}	0.0734	0.0679	7.5
Unsteady ξ_{tip}	0.0758	0.0700	7.7
% Difference	3.3	3.1	

Table 5.2: Impact of Unsteadiness on Time Average Tip Loss Coefficient

5.4 Analysis of Time Average Flow Field

The most important question to address for these unsteady calculations is how the presence of unsteadiness affects the time average solution because this influences the time average loss. The unsteady vane-blade interaction has an effect on the time average solution, but the results show the effects to be small which is in agreement with the small (3%) changes in time average tip loss coefficients.

5.4.1 Unsteady Time Average Blade Loading

The time average blade loading has an impact on the time average tip leakage flow magnitude, and the subsequent development into a tip leakage vortex. If there were changes in the average driving pressure gradient across the tip, we could expect changes in the leakage flow distribution. Our hypothesis is that if changes in the time average diffusion on the suction side of the blade near the trailing edge were present, the time average vortex structure would be impacted (assuming extreme

fluctuations are not present). Computations show there is little difference between the time average and the steady loading due to the presence of unsteadiness as illustrated by in Figure 5-5.

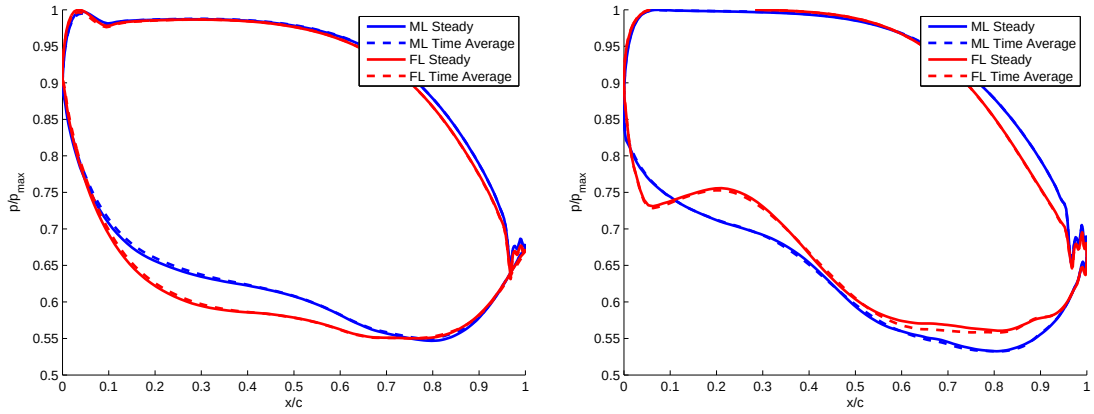

Figure 5-5: Steady and Unsteady Time Average Blade Loading Profiles a)50% span, 0% clearance, b)85% span, 2% clearance

5.4.2 Unsteady Time Average Leakage Massflow

Figure 5-6 shows the steady and time average leakage flow and leakage angle distributions, illustrating the changes in the unsteady results are small relative to the steady solution. This is expected because of the small changes in time average tip loading. The difference between the steady and time average massflow is discernible near the leading edge, but the difference in normalized leakage flow integrated over the tip gap is less than 0.1% as shown in Table 5.3.

	$\dot{m}_{main}$ (kg/s)	$\dot{m}_{tip}$ (kg/s)	Normalized $\dot{m}_{tip}$	% Change from Steady
ML Steady	0.485	0.0156	0.0323	
ML Unsteady	0.484	0.0156	0.0323	-0.026
FL Steady	0.483	0.0168	0.0349	
FL Unsteady	0.482	0.0168	0.0349	0.060

Table 5.3: Impact of Unsteadiness on Time Average Leakage Flow

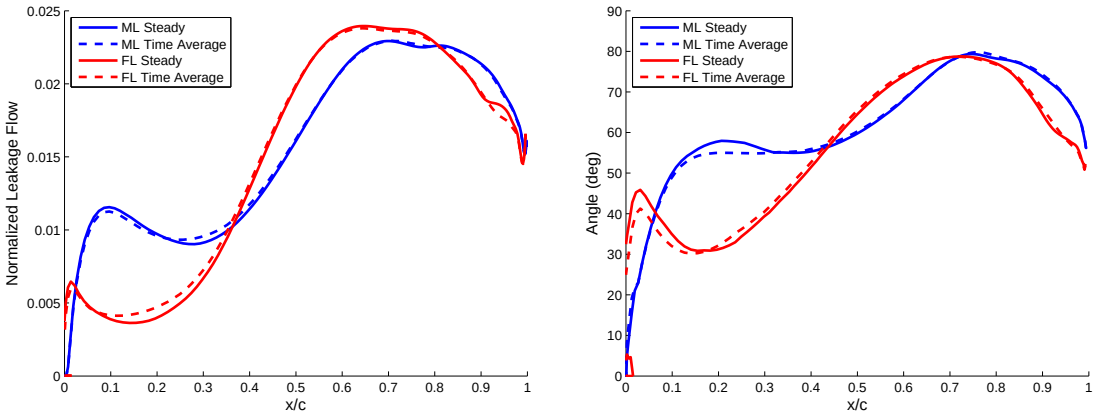

(a) (b)

Figure 5-6: Steady and Unsteady Time Average Leakage Flow Distributions: a)Leakage Mass Flow, b)Leakage Flow Angle

5.4.3 Unsteady Time Average Tip Leakage Vortex State

The details of the time average flow field provide information on the time average leakage flow mixing. The time average vortex properties can be expected to be similar to the steady properties because the tip loss increases by 3%. Post processing of the unsteady flow was done at 116 time intervals per cycle and then averaged. Figure 5-7 shows the core centerline velocity ratios versus axial distance. The velocity ratios match well between the computed steady flow field and the time average analysis, consistent with the small change in tip loss coefficient.

The axial distribution of time averaged dissipation in the vortex flow is shown in Figure 5-8. The ML blade has a larger dissipation peak in the breakdown region than the FL blade for both the steady and the time average results. The time average dissipation is close to the steady dissipation until the vortex reaches the breakdown location at x/c = 1.1. The total dissipation is about 10% lower between x/c = 1 and x/c = 2.5 for the unsteady time average cases compared to the steady cases. A possible explanation for the decrease in peak dissipation between unsteady time average and steady simulation results at this location is presented in Chapter 6.

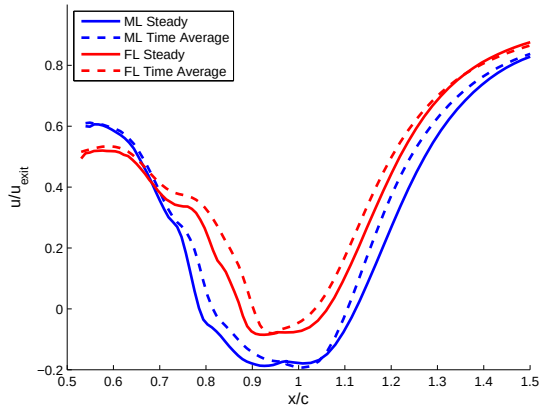

Figure 5-7: Steady and Unsteady Time Average Vortex Centerline Velocity Ratio

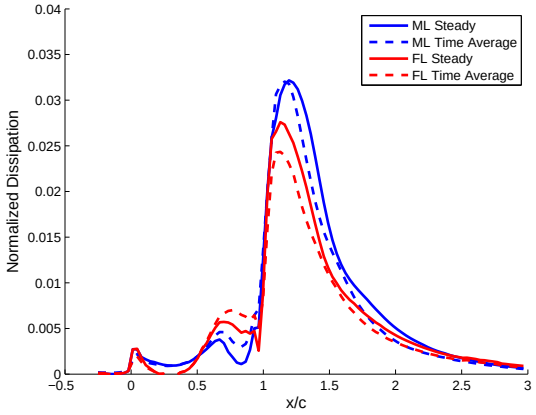

Figure 5-8: Steady and Unsteady Time Average Dissipation Due to Leakage Flow (2% case - 0% case), $NormalizedDissipation = \frac{d\xi}{d(x/c)}/c_p \Delta T_t$

5.5 Effect of High Amplitude Blade Loading Unsteadiness

As mentioned, the stage was also run with a modified vane that gave 2 blades for every 1 vane (airfoil counts: 29 vanes, 58 blades). The reason for this decision was to enable sliding plane calculations with fewer modeled blade passages to lower computation time. The level of unsteadiness increased because of the 2:1 count, resulting in larger blade loading fluctuations than with the design vane count. Figure 5-9 shows blade

loading envelopes (maximum variation at that location) of the amplitude versus axial distance for the original vane count and for the modified vane count cases. The modified vane count envelope is roughly twice the design vane count envelope at the radial station shown (75% span), and this trend was typical of the different span locations.

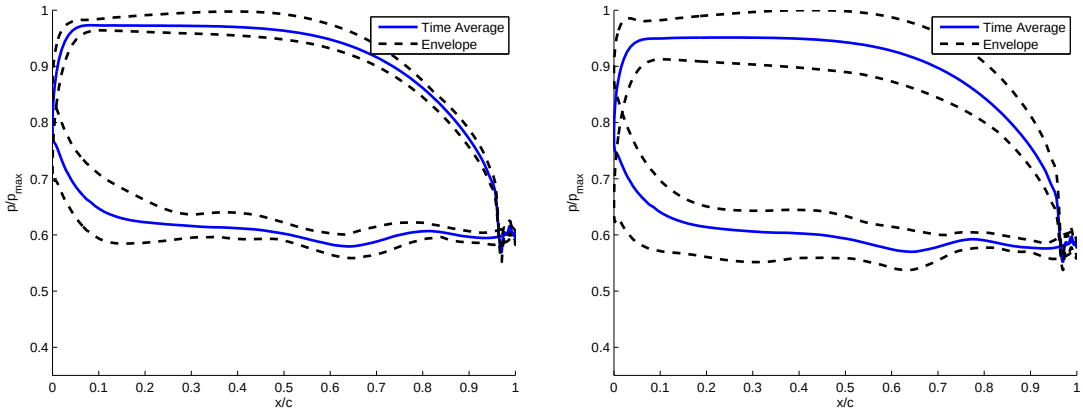

(a) (b)

Figure 5-9: Blade Loading Envelope Increases in Modified Count Case at 75% span: a)Original Case, b)Modified Case (2 blades for every 1 vane)

With these larger fluctuations in the modified count case, the time average tip loss coefficient also exhibits lower loss for the FL blade than the ML blade as shown in Table 5.5. The magnitude of tip loss coefficient change due to loading type is reduced from 7.3% to 6.0%. Table 5.4 shows the time average loss coefficient increases by about 4-9% due to the presence of unsteadiness, and is included for completeness. This more exteme case thus also agrees with the vortex in a pressure rise mechanism, with the implication that the findings are of more generic applicability.

	ML 0%	ML 2%	FL 0%	FL 2%
Steady ξ	0.0704	0.1437	0.0737	0.142
Unsteady ξ	0.0766	0.1493	0.0797	0.148
% Difference	8.9	3.9	8.2	4.5

Table 5.4: Impact of Unsteadiness on Time Average Stage Loss Coefficient: Modified 2 to 1 Blade Count

	ML	FL	% Change from ML Blade
Steady ξ_{tip}	0.0734	0.0679	-7.3
Unsteady ξ_{tip}	0.0727	0.0684	-6.0
% Difference	-0.9	0.5	

Table 5.5: Impact of Unsteadiness on Time Average Tip Loss Coefficient: Modified 2 to 1 Blade Count

5.6 Conclusions Concerning Time Average Results

The unsteady tip leakage flow due to an upstream nozzle guide vane has been examined computationally. The results of URANS computations show that reducing the pressure rise at the trailing edge has similar beneficial effects for unsteady flow as for steady flow. The time average loss coefficient increases roughly $4-5\%$, and the time average tip loss coefficient increases by about 3%, compared to the steady calculations. The time average properties show little change from the steady value with the exception of the dissipation associated with mixing of the leakage vortex, which was lower in the vortex breakdown region in the unsteady calculation by about 10% compared to the steady case. The benefit for changing blade tip geometry from a ML blade to a FL blade is thus valid in the presence of unsteadiness due to vane-blade interaction.

Chapter 6

Instantaneous Effects of Unsteady Upstream Vane Influence on Tip Leakage Vortex Mixing Losses

6.1 Introduction

In this chapter we examine the instantaneous effects of unsteadiness due to an upstream nozzle guide vane to provide insight into the time average results discussed in Chapter 5. The specific questions posed are:

- How does the leakage flow distribution fluctuate with time?
- How does the vortex flow field fluctuate with time?
- How does the loss generation respond as a result of the above temporal fluctuations?
- How generic are the conclusions that we can draw?

6.2 Characterization of Unsteady Behavior Due to Vane Passing

Despite the small changes in time average tip leakage loss and leakage flow properties, the changes within a vane passing period are substantial. It is thus useful to examine the "cause" of the small time average changes. The role of unsteadiness in the flow field can be examined from the one-dimensional momentum equation for inviscid flow, Equation 6.1.

$$\frac{\partial u}{\partial t} + u\frac{\partial u}{\partial x} = \frac{dp}{dx} \tag{6.1}$$

Equation 6.1 shows the pressure gradient is balanced by the sum of the local and convective accelerations. The ratio of the two terms is represented by the reduced frequency, which would be defined for this comparison as $\beta = {}^{(\partial u/\partial t)}/_{(u\partial u/\partial x)}$. The reduced frequency of a system can also be defined more globally, using representative values as $\beta = {}^{\omega L}/_{U}$. L is a relevant length scale of the system, U is a representative flow-through velocity, and ω is a representative frequency of the unsteadiness source. The reduced frequency can be thought of as the ratio of the flow-through time to the flow-change time, and the behavior of an unsteady flow can be classified based on the reduced frequency magnitude [6].

$\beta \ll 1$ unsteady effects small - quasi-steady flow;

$\beta \gg 1$ unsteady effects dominate;

$\beta \sim 1$ both unsteady and quasi-steady effects important;

For an axial flow turbine, the reduced frequency due to blade or vane passing is typically of order one [6]. If the characteristic velocity is chosen to be the average axial velocity in the blade passage and the characteristic length is taken to be the

blade axial chord, β for the present stage is 0.8.

A local reduced frequency can also evaluated as a point quantity in the flow field by examining the ratio of the local and convective accelerations, defined as $\beta_{acc} = |\partial\vec{v}/\partial t|/|\vec{v}d\vec{v}/d\vec{x}|$. (In doing this calculation of reduced frequency included all acceleration terms, not just those in the axial direction.) The reduced frequency calculated in the flow field, spatially averaged versus axial location and then time averaged, is shown in Figure 6-1. The three curves are the β_{acc} in the upper 50% of the passage, the β_{acc} outside the vortex core in the upper 50% of the passage, and the β_{acc} inside the vortex core. The figure shows increased unsteadiness inside the vortex core, which peaks at the trailing edge. This agrees with the high velocity gradients due to the swirling flow and the core reversal region. Small changes in the vortex centerline location can create local accelerations.

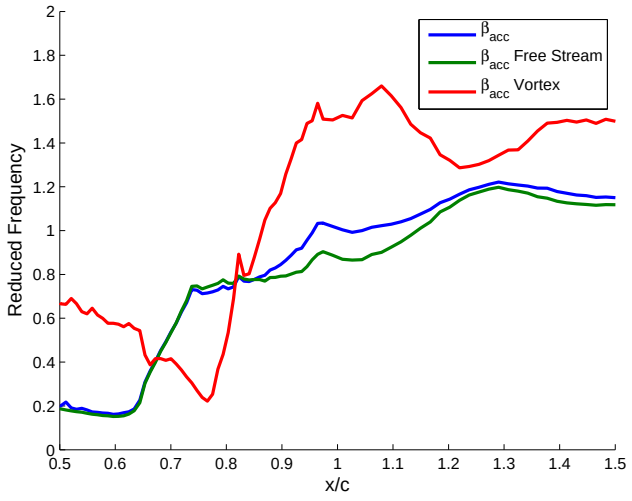

Figure 6-1: Unsteady Time Average Reduced Frequency, Spatially Averaged Perpendicular to Streamwise Direction, ML Blade 2% Clearance

The passage reduced frequency based on characteristic values and the flow field time average reduced frequency for the tip leakage vortex flow are both of order unity, so both steady and unsteady effects are important. For the flow through the gap however, using the average gap velocity and average blade tip width, gives a calculated value of β to be 0.07. This is an order of magnitude smaller than the

freestream value and implies the gap flow regime is quasi-steady.

6.3 Analysis of Instantaneous Flow Field

6.3.1 Unsteady Tip Leakage Massflow

The magnitude of the tip leakage flow is a contributor to the tip leakage loss, and we now examine its time variation. There are temporal changes in leakage flow due to the temporal variations in blade tip loading. Figures 6-2(a) and 6-2(b) show the pressure envelopes (p versus x/c) at 75% span for the ML and FL blades respectively. These illustrate the maximum and minimum pressures at each spatial location on the blade over the period. The figures illustrate that the amplitude of the fluctuations is greatest on the suction side of the blade and the unsteadiness is concentrated toward the blade leading edge.

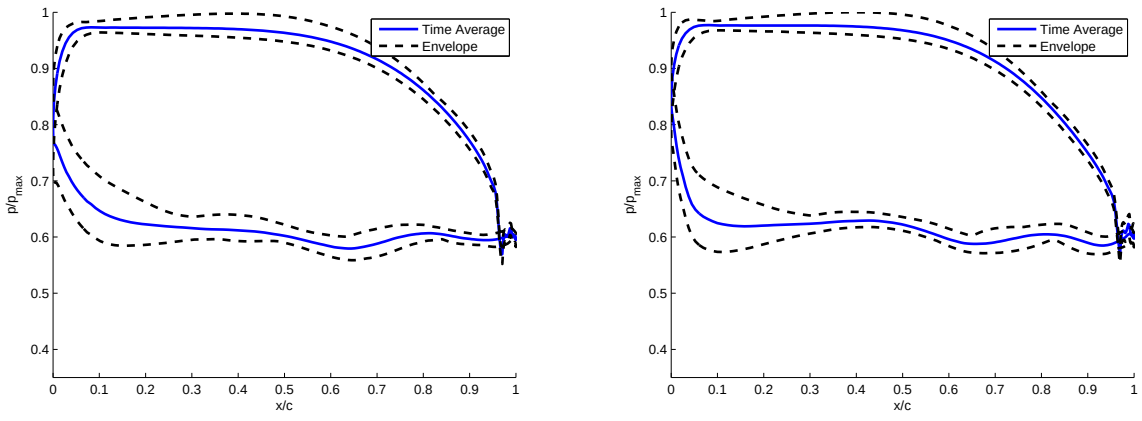

(a) (b)

Figure 6-2: Blade Loading Envelopes at 75% span, 2% clearance: a)ML blade, b)FL blade

Due to the blade pressure fluctuations, the leakage flow through the gap also varies with time. Figure 6-3(a) illustrates the tip leakage massflow distribution envelope, the maximum and minimum leakage flow at any given time, versus gap exit location. Figure 6-3(b) illustrates the amplitude in leakage flow of the fluctuation, taken to

be the difference of the maximum and minimum envelope curves normalized by the axial stage massflow, versus gap exit location. The amplitude of unsteadiness is concentrated towards the leading edge and decays towards the trailing edge. Figure 6-4 shows analogous graphs of the leakage flow angle, measured from the streamwise direction. The maximum variation is 20° and is concentrated towards the leading edge.

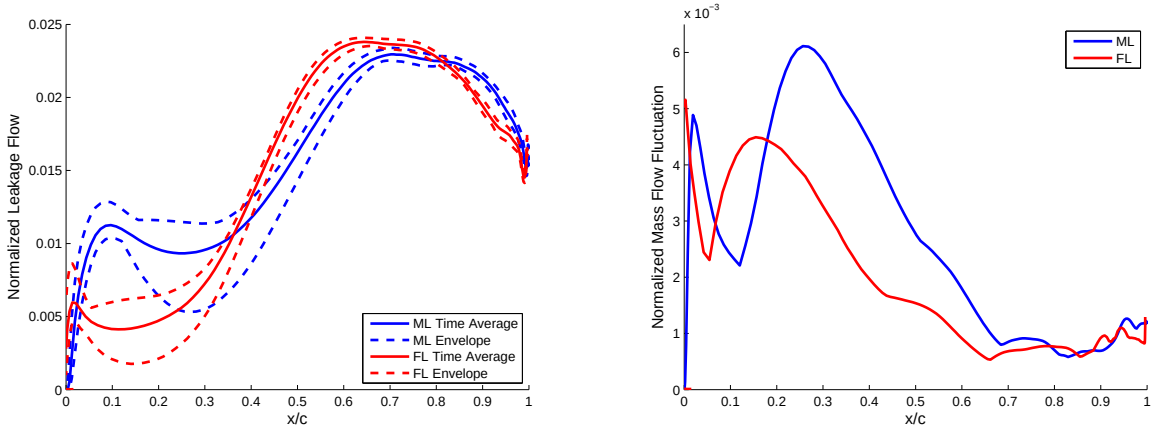

(a) (b)

Figure 6-3: Unsteady Tip Leakage Flow: a)Leakage Mass Flow Envelope, b)Amplitude of Fluctuations

The quasi-steady gap flow assumption, implied by the evaluation of the gap reduced frequency, is next assessed. The driving pressure difference across the tip is approximated as the instantaneous blade tip loading (taken to be the integrated pressure difference between the pressure and suction side of the blade at 85% span). Figure 6-5 shows the time variation of the blade tip loading and leakage flow are roughly in phase, supporting the quasi-steady gap flow approximation.

To further assess the quasi-steady approximation we can compare a quasi-steady leakage flow analysis to the computed leakage flow. The quasi-steady analysis used a steady upstream stagnation pressure, the average gap discharge coefficient, and the unsteady instantaneous suction side blade pressures at 85% span to provide the axial distribution of quais-steady gap leakage flow. This leakage distribution was integrated to yield the quasi-steady leakage flow at each instant. Figure 6-6 shows

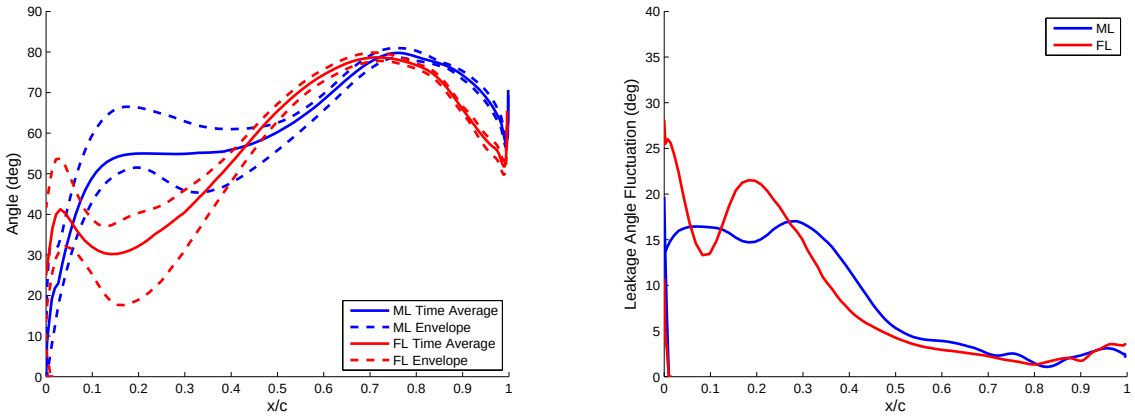

(a) (b)

Figure 6-4: Unsteady Tip Leakage Angle: a)Leakage Flow Angle Envelope, b)Amplitude of Fluctuations

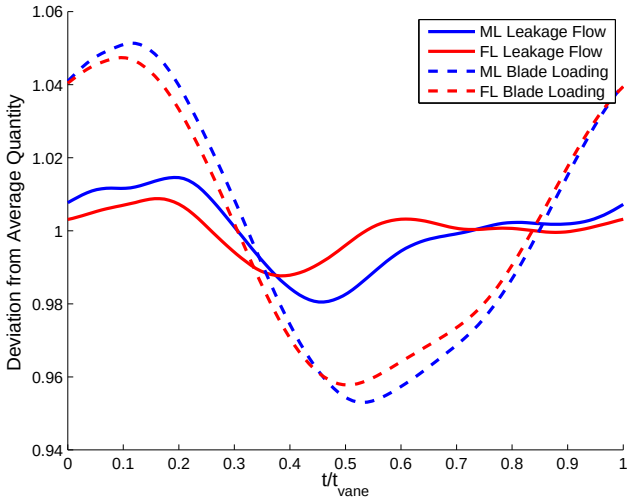

Figure 6-5: Time Variation of Tip Leakage Flow and Tip Blade Loading

the quasi-steady leakage flow to be in phase with the computed leakage flow from the numerical simulations. The time average quasi-steady leakage flow differs by 1.5% from the CFD tip leakage flow, supporting the quasi-steady nature of the gap flow.

It is worth noting that the time variation in integrated blade loading is smaller than that implied by the unsteady pressure amplitude in the blade loading envelope. This is because the loading does not increase or decrease across the entire blade chord

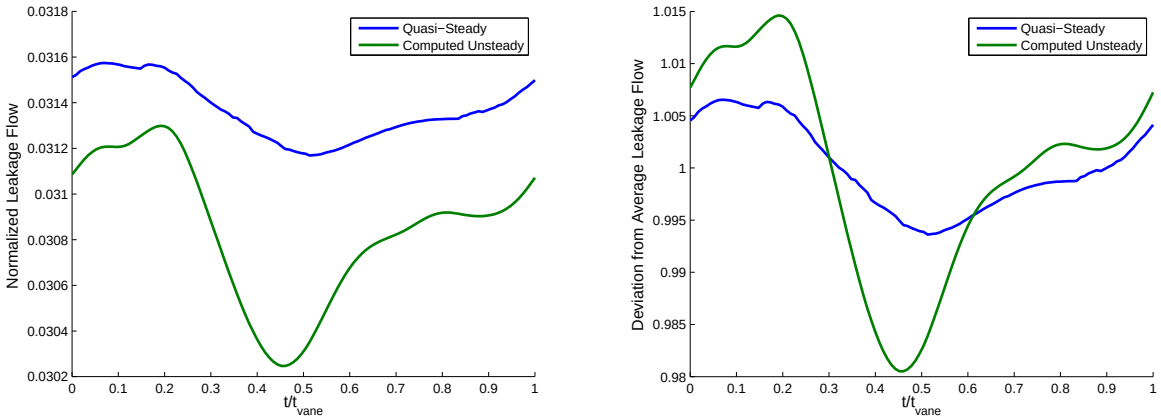

(a) (b)

Figure 6-6: Comparison of Time Variation of Quasi-Steady and Actual Leakage Flow: a)Normalized Leakage Flow: $\dot{m}_{tip}/\dot{m}_{main}$ b)Normalized by Mean Leakage Value: $\dot{m}_{tip}/\dot{m}_{tipavg}$

in phase. Figure 6-7 illustrates this point. The instantaneous blade loading and the mass flow distribution are given as a function of x/c, at two instants in time.

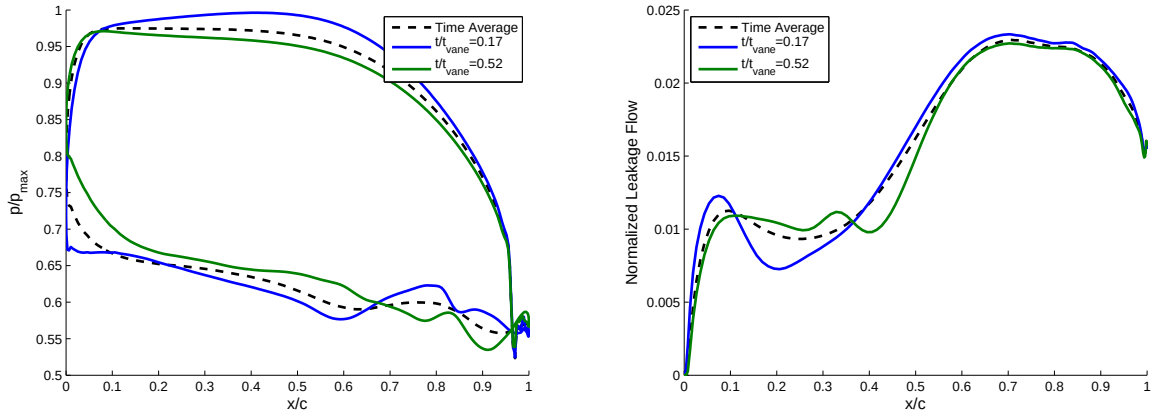

(a) (b)

Figure 6-7: Instantaneous Pressure and Leakage Flow Behavior: a)Snapshots of ML Blade Loading at 85% Span, b)Snapshots of Leakage Flow Distribution

The instantaneous pressure exceeds the mean value at some locations on the blade, but is lower than the mean at others. The result is an integrated variation in pressure substantially lower than the blade loading envelope suggests. If the extremes of the

blade loading envelope were used, the total loading would vary ±15% from the mean loading, instead of the ±6% result obtained by computing the loading at each instant in time. The temporal mass flow variation calculated from the numerical simulation is thus also smaller than if it were based on the leakage flow envelope. Using the extremum of the leakage flow envelope, the variation would be ±8% from the mean leakage flow, instead of the ±1.5% result from the numerical simulations.

6.3.2 Unsteady Tip Leakage Vortex State

The tip clearance vortex, and therefore the loss generated by the leakage flow, experiences considerable fluctuations due to unsteady vane passing. The core velocity ratio, circulation, vortex area, and core stagnation pressure all fluctuate, as does the pressure rise to which the core is subjected.

To characterize the unsteadiness, the average core velocity ratio envelope is shown in Figure 6-8 for axial locations between x/c = 0.7 and x/c = 1.5. The core experiences ±15% variation in the time average core velocity in the breakdown region at x/c = 1.05.

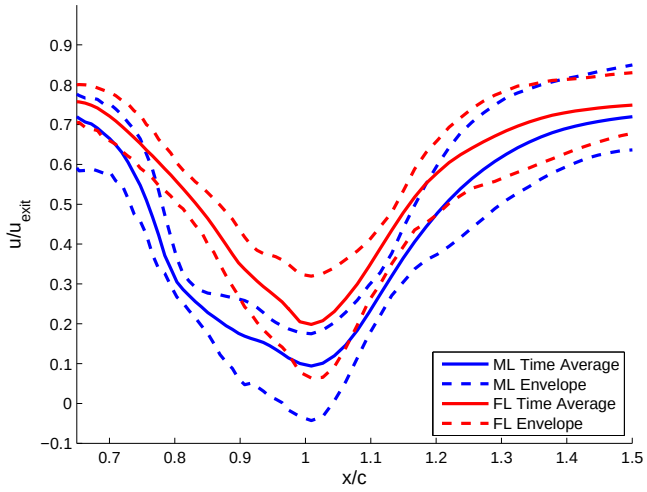

Figure 6-8: Unsteady Vortex Core Velocity Ratio Envelope

Figure 6-9 illustrates the time variation of the spatially averaged pressures inside

the vortex core and in the passage outside the vortex core at x/c = 0.7. The pressure fluctuations within the core are in phase with changes in the pressure external to the core, thus the external pressure drives the core pressure. Similar analyses at other locations in the range x/c = 0.7 to x/c = 1.4 also show the core and passage pressures are in phase.

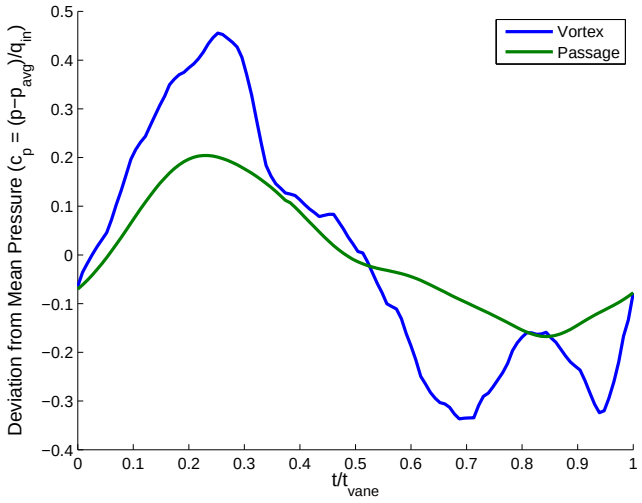

Figure 6-9: Time Variation of Pressures, Spatially Averaged Perpendicular to Streamwise Direction at x/c = 0.7: Inside Vortex Core and External to Vortex Core in Upper 50% Span of Passage

6.3.3 Unsteady Loss Generation

The instantaneous dissipation field was assessed to determine the impact of vortex flow field fluctuations on the time variation of leakage loss generation. Figure 6-10 gives a dissipation envelope, which shows the extremum over the period of the integrated dissipation on axial slices in the blade passage for the 2% clearance case minus the 0% clearance case. The figure illustrates the variation in loss generation is concentrated in the vortex breakdown region from x/c = 1.1 to x/c = 1.7. The mixing loss scales with $(\Delta u)^2$, and this region is also the location of the largest Δu between the core and freestream, within which the minimum core velocity exists.

Figure 6-11 captures the time variation of loss generation in the breakdown region,

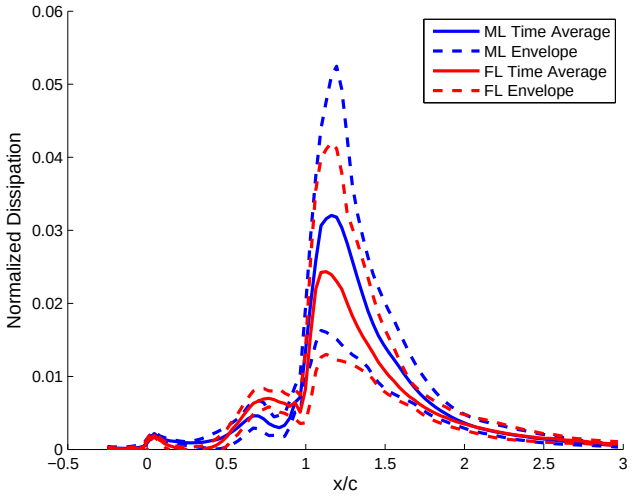

Figure 6-10: Leakage Loss Generation Envelope (2% case - 0% case): $NormalizedDissipation = \frac{d\xi}{d(x/c)}/c_p \Delta T_t$

showing the total dissipation in the control volume enclosing the breakdown region (displayed in Figure 5-3(b)). The variations of the entropy production due to the vortex breakdown are approximately ±20% compared to the mean volume total dissipation. The ML and FL blades loss generation behave in a similar manner, in that they are in phase with one another and have similiar magnitudes of time variation amplitude.

To determine why these large variations are present, the time variation of the breakdown control volume average velocity deficit in the core was examined. In Figure 6-12, the velocity deficit, Δu, is defined to be the difference in streamwise velocity between any point inside the vortex core and the average velocity outside the core at each axial slice in the breakdown control volume. The figure shows that the volume average velocity deficit is shown to vary by ±15% from the time average volume average deficit. This magnitude of variation is similar both to what was seen in the core velocity envelope in Figure 6-8, and to the breakdown control volume dissipation variation illustrated in Figure 6-11.

Comparison of Figure 6-11 and Figure 6-12 shows that the time variation of velocity deficit leads the dissipation inside the breakdown control volume by roughly 1/6

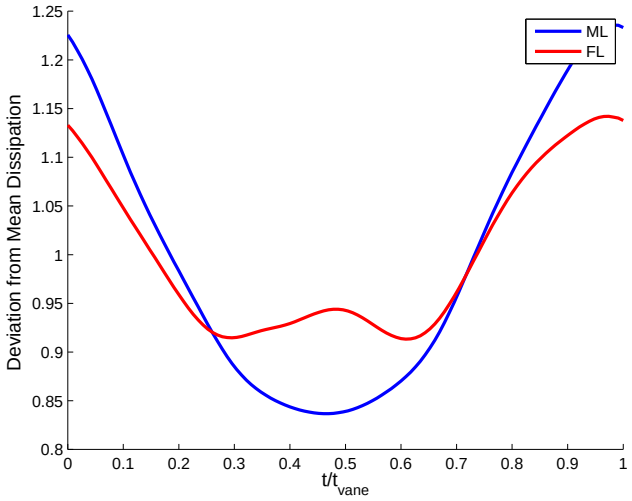

Figure 6-11: Time Variation of Spatially Averaged Vortex Loss Generation in Breakdown Control Volume

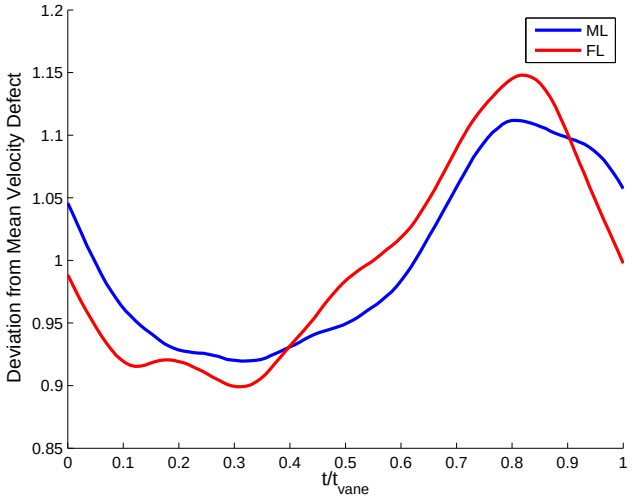

Figure 6-12: Time Variation of Spatially Averaged Streamwise Velocity Defect of Vortex Core in Breakdown Volume

vane passing periods. The reason for the phase offset can be explained using the dissipation equation, Equation 6.2. We can break the dissipation into two parts, namely the factor of $^{2\mu_{eff}}/_{T}$, and the velocity gradient terms. Figure 6-13 shows the time variation of these two parts, spatially averaged over the breakdown control volume.

$$\rho\frac{ds_{visc}}{dt} = \left(\frac{2\mu_{eff}}{T}\right)\left[\left(\frac{du}{dx}\right)^2 + \left(\frac{dv}{dy}\right)^2 + \left(\frac{dw}{dz}\right)^2 + \frac{1}{2}\left(\frac{du}{dy} + \frac{dv}{dx}\right)^2 + \frac{1}{2}\left(\frac{du}{dz} + \frac{dw}{dx}\right)^2 + \frac{1}{2}\left(\frac{dv}{dz} + \frac{dw}{dy}\right)^2 - \frac{1}{3}\left(\frac{du}{dx} + \frac{dv}{dy} + \frac{dw}{dz}\right)^2\right] \tag{6.2}$$

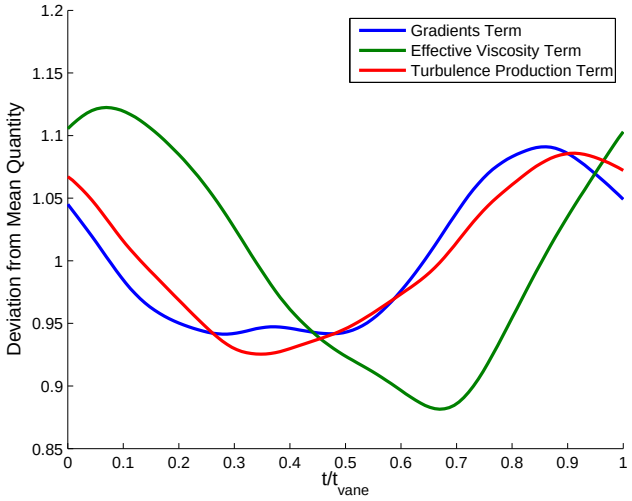

Figure 6-13: Time Variation of Spatially Averaged Dissipation Decomposition Terms and Turbulence Production in Breakdown Control Volume

Comparison of Figure 6-13 and Figure 6-12 shows the gradients inside the control volume are in phase with the vortex core velocity deficit. However, the viscosity term lags behind by roughly 1/4 periods. The reason for the phase offset between the viscosity and gradient terms can be explained using the turbulence production, S, in Equation 6.3 [2].

$$S = \sqrt{2\Omega_{ij}\Omega_{ij}} - 2.0min(0, \sqrt{2S_{ij}S_{ij}}) - \sqrt{2\Omega_{ij}\Omega_{ij}}) \tag{6.3}$$

The time variation of the spatially averaged turbulence production in the control volume is shown in Figure 6-13 to be in phase with the gradient terms. The turbulence production S, rather than the actual viscosity μ_{eff}, is in phase with the gradient terms. Thus, the dissipation lags the velocity deficit signal. The decrease in time

average breakdown dissipation due to unsteadiness, in Figure 5-8, is thus caused by the lag between the turbulent viscosity and velocity gradients.

6.3.4 Source of Time Variation in Leakage Flow Loss Generation

Two sources of the unsteady loss generation variation exist. One is the temporal variation in tip gap exit flow. The second is temporal alteration of the vortex breakdown severity. To determine whether one source is dominant, we have carried out a control volume analysis to mix out the gap exit flow at constant pressure for every time step during the period. The time average distribution of normalized loss contribution resulting from this analysis (calculated with Equation 3.1) versus axial distance along the gap is shown in Figure 6-14. The time average mixing loss integrated over the gap has a 7.5% and 5.5% increase for the ML and FL cases respectively compared to the steady flow computations.

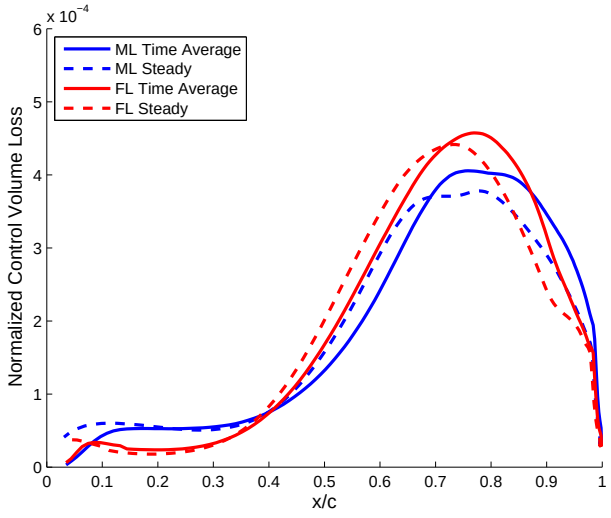

Figure 6-14: Steady and Time Average Loss Distribution with Leakage Flow Mixed Out at Instantaneous Suction Side Pressure, $Normalized\ CVloss = {}^{T_e ds}/_{c_p \Delta T_t}$

The time variation of the gap exit control volume loss, integrated over the blade axial chord, is shown in Figure 6-15. Two aspects of the flow can be seen. First,

comparison of Figure 6-15 and Figure 6-5 shows the unsteady control volume loss is roughly in phase with the magnitude of the tip leakage flow, because higher massflow corresponds to higher cross flow velocity which means more lost kinetic energy. Second, the variation of the gap exit control volume loss is roughly ±6%, considerably lower than the ±20% variation in unsteady loss generation in the vortex breakdown region. The implication is that the major contributor to time variation in tip leakage flow loss generation is the time variation in the pressure field to which the vortex is exposed, not the time variation in unsteady tip leakage flow.

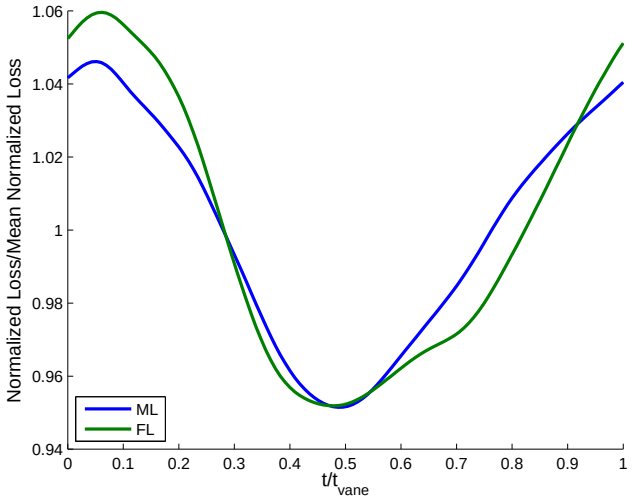

Figure 6-15: Time Variation of Leakage Loss for Gap Flow Mixed Out at Constant Instantaneous Pressure

6.4 Comments on Generic Flow Features

To provide insight into the three-dimensional turbine calculation results an axisymmetric model problem has been examined to determine the loss behavior of an unsteady vortex. These calculations also enable comments to be made concerning the generic applicability of the conclusions regarding the time average results in Chapter 5. The model problem is a vortex in a time varying pressure rise. The source of unsteadiness was selected because the pressure rise a vortex experiences is central to the steady vortex breakdown mechanism.

6.4.1 Computational Details

The axisymmetric CFD was done in FLUENT as in the work of Huang who characterized the behavior of vortices in a pressure rise [9]. The configuration was a diverging duct, with inlet stagnation pressure distribution corresponding to a Burger's vortex. The exit boundary condition was specified as a simple radial equilibrium static pressure distribution with the pressure at vortex centerline at the duct exit specified in time (as a user defined function in FLUENT)[1]. The outer wall is a slip wall to avoid extraneous losses, and the Re-Normalisation Group (RNG) $k-\epsilon$ turbulence model was used.

The axial and swirl velocity inlet profiles for the axisymmetric vortex are given in Figure 6-16 as a function of radius normalized by the core edge radius. The swirl number at the inlet was set to 0.83 and the inlet core velocity defect was 0.6, as in the vortex about 0.2 axial chords upstream of vortex breakdown in the three-dimensional turbine case.

A sample grid is shown in Figure 6-17 to illustrate the axial distances in the geometry. The radius of the duct is 10 times that of the vortex core (r_e). The vortex radius approximately matches (within 25%) the radius of the tip leakage vortex at

[1]Calculations were also done with inlet velocity fluctuations corresponding to variations in velocity defect and in circulation. These did not capture the behavior seen in the three-dimensional calculations and they have not been included here. The total variation in time average mixed out loss with these calculations differed less than 10% compared to steady cases for unsteadiness amplitudes as high as 40%.

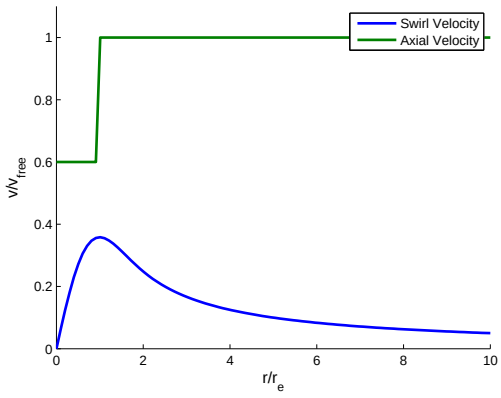

Figure 6-16: Axisymmetric Vortex Inlet Velocity Profiles: Axial Velocity Core Defect = 0.6, Swirl Number = 0.83

x/c = 0.74, upstream of the breakdown location. The freestream axial velocity, unsteady period, and axial system length were specified as a group to ensure the model computations had a similar reduced frequency to the three dimensional turbine computations.

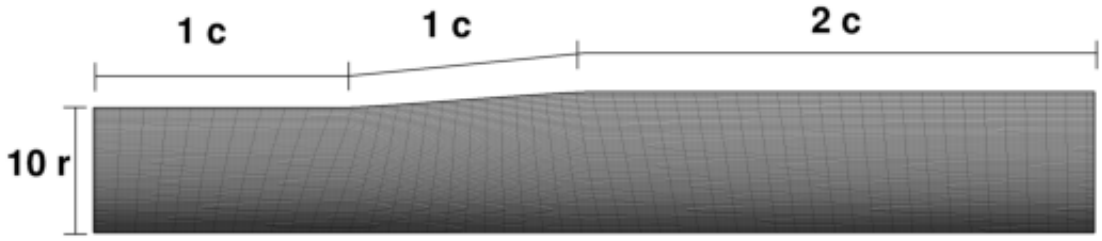

Figure 6-17: Axisymmetric Vortex Computational Domain

6.4.2 Loss Mechanisms for a Vortex in an Unsteady Pressure Rise

For a steady tip leakage vortex, Huang showed that the vortex mixing loss can decrease with increase in pressure rise, but at the onset of vortex breakdown the loss increases rapidly with increase in pressure rise [9]. To make a general statement that this scenario holds in unsteady flow, we need to show the behavior is replicated in a flow with a time varying pressure rise. The magnitude of the pressure rise in the steady

axisymmetric cases, and the time average pressure rise in the unsteady calculations (over the range of parameters studied), is set by the duct area ratio. To assess the vortex mixing loss mechanism in unsteady flow, a range of duct area ratios from 1 to 1.32 were used to provide C_p values ranging from 0 to 0.42. Three separate cases were run: steady flow, unsteady flow with exit pressure variation of $\pm 10\%$, and unsteady flow with exit pressure variation of $\pm 20\%$ from the mean C_p.

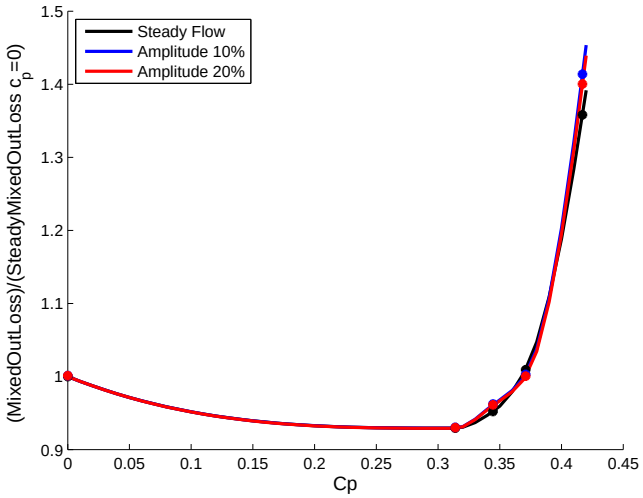

Figure 6-18: Mixed Out Loss for a Vortex in Unsteady Flow in a Pressure Rise

Figure 6-18 shows mixed out loss versus pressure rise for steady and time average unsteady cases. The difference between the mixed out loss of the time average unsteady flow and the steady flow is roughly 1%. The small changes in loss are due to the low curvature shape of the loss vs. C_p curve; it is essentially two linear sections connected by a "knee" which corresponds to the onset of vortex breakdown. The impact of the unsteady pressure variation should be most pronounced in the high curvature region with $C_p = 0.35$.

The unsteadiness was further examined in two sets of calculations with fixed duct geometry corresponding to $C_p = 0.35$. The first set was designed to examine the sensitivity of the time average mixed out loss to the unsteady pressure amplitude. The second set assessed the impact of reduced frequency on the time average mixing loss. Figure 6-19, which shows mixing loss versus exit pressure amplitude (normalized

by the time average C_p), illustrates the small sensitivity of the mixed out loss to the unsteady pressure rise fluctuations. Figure 6-20 shows the variation in loss versus reduced frequency (normalized by the β for the three-dimensional case). Again, there is only a small variation in loss. In summary, neither a time variation of exit pressure of $\pm 40\%$, or an order of magnitude change in reduced frequency result in more than a 2% increase in mixed out loss relative to steady flow.

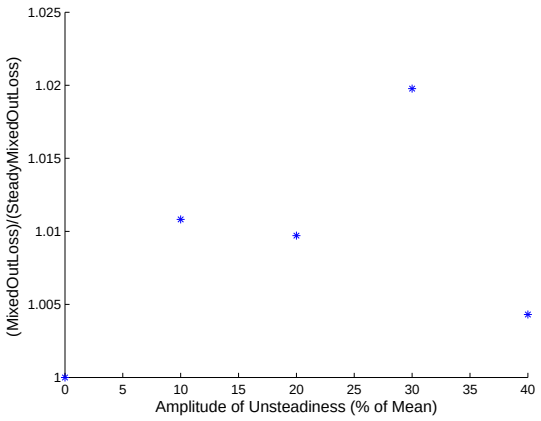

Figure 6-19: Sensitivity of Time Average Mixing Loss to Amplitude Variation

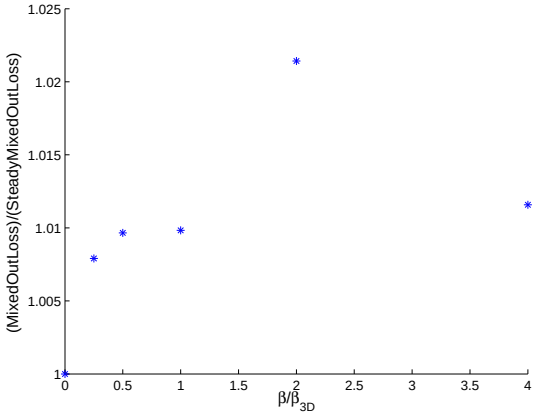

Figure 6-20: Sensitivity of Time Average Mixing Loss to Reduced Frequency Variation

6.5 Conclusions

Instantaneous leakage flow changes in the unsteady flow have been assessed to provide insight for the time average results. Consideration of the reduced frequency showed that both steady and unsteady effects are important for the vortical flow, although the flow through the gap is quasi-steady. The quasi-steady assumption for gap flow was further supported by comparisons of the quasi-steady leakage flow and the leakage flow from the numerical simulations.

The streamwise velocity in the core shows fluctuations of $\pm 15\%$ and these fluctuations were shown to be associated with loss generation variations of similar size. Comparison of the time variations of loss generation and of gap exit control volume loss shows that the unsteady change in pressure rise experienced by the vortex plays the dominant role in driving the fluctuations in the vortex breakdown region.

To provide insight concerning the applicability of the vortex breakdown loss mechanism in an unsteady flow, a model problem of an axisymmetric vortex in an unsteady pressure rise was examined. The behavior of the unsteady vortex mixing loss matched the steady flow loss mechanism; mixing loss decreases with increasing pressure rise until the onset of vortex breakdown. In addition, the mixed out loss was shown to be insensitive (less than 2% change) to pressure rise fluctuation amplitudes of $\pm 40\%$ compared to the mean C_p and order of magnitude changes in reduced frequency. The results imply that time average tip loss behaves similar to the steady calculations not only for this turbine, but for similar turbine designs as well.

Chapter 7

Conclusions and Recommendations for Future Work

7.1 Summary

Three dimensional RANS and URANS calculations have been used to assess the impact of several specific design features and aspects of the actual turbine environment on turbine blade tip loss mechanisms. In particular, examination was carried out of the effects of bowing (positive and negative), the effect of downstream transition duct geometry, and the effect of unsteadiness due to an upstream vane. A summary of the results is given below.

- Tip clearance loss is reduced by positive blade bow. A blade with the two-dimensional airfoil sections shifted tangentially such that the suction side is radially concave reduces the tip loss coefficient. Loss is reduced due to reduction of the tip loading, which decreases the velocity difference between leakage flow and suction side passage flow, and hence the mixing losses. The maximum positive bow studied in this work was 130°, resulting in a 20% reduction in the tip loss coefficient.

- Over the range examined, the effect of the downstream diffusing transition duct design on tip leakage losses is small compared to the effect of changing the blade

tip design. A 65% increase in duct area ratio caused a 3.6% increase in tip loss coefficient. In contrast, the change in geometry between a mid loaded blade and a forward loaded blade created a 7.5% decrease in tip loss. There are two reasons for this. One is the difference in vortex state, in that the diffusing duct acts on the vortex when it has low swirl and high ratio of core to freestream velocity (S $\sim$ 0.2 and VR $\sim$ 0.7 in the case investigated). Blade geometry design affects the vortex at high swirl and low ratio of core to freestream velocity (S $\sim$ 1.2, VR $\sim$ 0.2 in the case investigated). The latter condition is much more sensitive to changes in pressure than the former. In addition, the variation in pressure gradient between duct designs is an order of magnitude less than for variations due to blade geometry design. The implication is that the downstream diffusing transition duct can be designed to meet other constraints without creating large increases in tip loss.

- The time average tip leakage loss calculated using URANS, with unsteadiness arising from the upstream nozzle guide vane, differed less than 5% from tip leakage loss calculated on a steady state basis. The time average blade loading, leakage flow, and vortex core velocity also show little change relative to steady state calculations. Further, model calculations with an axisymmetric vortex show the tip leakage loss vortex breakdown mechanism is insensitive to unsteady pressure fluctuations, at least up to an amplitude of $\pm$40% of the mean pressure rise. This implies that steady calculations can provide tip loss coefficient trends adequately.

- The reduced frequency of the vortical flow was 0.8. The tip gap flow, however, is characterized by a reduced frequency less than 0.1, and can be treated as quasi-steady, as verified by comparison of quasi-steady gap flow analyses to the unsteady computations.

- Although the time average quantities match the steady values, there are substantial instantaneous fluctuations in the vortex flow field. The vortex core velocity in the breakdown region changes by $\pm$15% over the period, causing

variation in the breakdown dissipation of ±20%. The reason for these variations is the gap flow does not mix out instantly, but forms a vortex that is subjected to a time-varying pressure rise at the blade trailing edge; if the leakage flow did mix out instantly, the loss generation would vary by ±6%. The disparity between the unsteady variation in actual loss generation and loss generation estimation due to instantaneous mixing is analagous to the scenario previously described by Huang for steady flow; it is important to the instantaneous loss generation that the leakage flow creates a tip leakage vortex which only mixes out after passing through a pressure rise in the region of the blade trailing edge.

- Based on the computations, the mechanism for tip leakage vortex loss in the three different situations examined appears to be similar to that which is seen for an isolated turbine blade.

7.2 Recommendations for Future Work

A next step in this research could be to determine the effect of the downstream vane passing pressure field on the tip leakage vortex, and the subsequent mixing loss. Following this, an unsteady 1.5 stage study should be run to determine if there are interaction effects between the two sources of unsteadiness. It is possible that benefits could be realized by clocking the downstream vanes relative to the upstream vanes.

In addition, a steady parametric analysis of inlet conditions on the tip leakage loss generation would be useful. The impact of boundary layer thickness on vortex formation is a feature that should be quantified.

Finally, in connection with the overall problem of unsteady loss and mixing, it would be useful to define the effect of vane-blade interaction on wake mixing and loss for a basic case such as a two-dimensional flow.

Bibliography

[1] T.C. Booth. Importance of tip clearance flows in turbine design. In *Tip Clearance Effects in Axial Turbomachines*, VKI Lecture Series. VKI, 1985.

[2] J. Dacles-Mariani, G. G. Zilliac, J.S. Chow, and P. Bradshaw. Numerical/experimental study of a wingtip vortex in the near field. *AIAA Journal*, 33(9):156101568, 1995.

[3] J.D. Denton. Loss mechanisms in turbomachines. *Journal of Turbomachinery*, 115:621–656, 1993.

[4] J.D. Denton and L. Xu. The exploitation of three-dimensional flow in turbomachinery design. *Journal of Mechanical Engineering Science*, 213:125, 1998.

[5] S. Gegg. Personal Communication, 12 Dec. 2011.

[6] E.M. Greitzer, C.S. Tan, and M.B. Graf. *Internal Flow, Concepts and Applications*. Cambridge University Press, 2004.

[7] N.W. Harvey. Aerothermal implications of shroudless and shrouded blades. In *Turbine Blade Tip Design and Tip Clearance Treatment*, VKI Lecture Series. VKI, 2004.

[8] F.J.G. Heyes and H.P. Hodson. The measurement and prediction of the tip clearance flow in linear turbine cascades. *Journal of Turbomachinery*, 115:376–382, 1993.

[9] A. C. Huang, E. M. Greitzer, C. S. Tan, E. F. Clemens, S. G. Gegg, and E. R. Turner. Blade loading effects on axial turbine tip leakage vortex dynamics and loss. Number GT2012-68302 in Turbo Expo, Copenhagen,Denmark, June 2012. ASME.

[10] M.Yaras and S.A. Sjolander. Prediction of tip-leakage losses in axial turbines. *Journal of Turbomachinery*, 114:204–210, 1992.

[11] G. Sovran and E.D. Klomp. Experimentally determined optimum geometries for rectininear diffusers with rectangular, conical or annular cross-section. *Fluid Mechanics of Internal Flow*, 1967.

[12] J.B. Staubach, O.P. Sharma, , and G.M. Stetson. Reduction of tip clearance losses through 3-d airfoil designs. Turbo Asia, Jakarta, Indonesia, Novmeber 1996. ASME.

[13] Jesse Wells. Effects of turbulence modeling on rans simulations of tip vortices. Master's thesis, Virginia Polytechnic Institute and State University, 2009.

[14] B. Liu Y. Liu, X. Yu. Turbulence models assessment for large-scale tip vortices in an axial compressor rotor. *Journal of Propulsion and Power*, 24, 2008.